Journal of Biological Chemistry. (2007) 282(47): 34429-34447.

Critical Role of Glu^<40>-Ser^<48> Loop Linking Actuator Domain and First Transmembrane Helix of Ca^<2+>-ATPase in Ca^<2+> Deocclusion and Release from ADP-insensitive Phosphoenzyme.

Daiho T, Yamasaki K, Danko S, Suzuki H.

Critical Role of Glu^{40}-Ser^{48} Loop Linking Actuator Domain and 1st Transmembrane Helix of Ca^{2+}-ATPase in Ca^{2+} Deocclusion and Release from ADP-insensitive Phosphoenzyme*

Takashi Daiho[1], Kazuo Yamasaki, Stefania Danko, and Hiroshi Suzuki

From the Department of Biochemistry, Asahikawa Medical College, Asahikawa 078-8510, Japan

RUNNING TITLE: ADP-insensitive Phosphoenzyme with Occluded Ca^{2+} in SERCA1a

[1] Address correspondence to: Dr. Takashi Daiho, Dept. of Biochemistry, Asahikawa Medical College, Midorigaoka-higashi, Asahikawa, 078-8510, Japan. Tel.: +81 166 68 2350; Fax: +81 166 68 2359; E-mail: daiho@asahikawa-med.ac.jp.

Functional importance of the length of the A/M1-linker (Glu^{40}-Ser^{48}) connecting the Actuator domain and 1st transmembrane helix of sarcoplasmic reticulum Ca^{2+}-ATPase was explored by its elongation with glycines-insertion at Pro^{42}/Ala^{43} and Gly^{46}/Lys^{47}. Two or more glycines-insertion at each site completely abolished ATPase activity. The isomerization of phosphoenzyme intermediate (*E*P) from the ADP-sensitive form (*E*1P) to ADP-insensitive form (*E*2P) was markedly accelerated but the decay of *E*P was completely blocked in these mutants. *E*2P thus accumulated was demonstrated to be *E*2PCa_2 possessing two occluded Ca^{2+} ions at the transport sites, and the Ca^{2+} deocclusion and release into lumen was blocked in the mutants. By contrast, the hydrolysis of the Ca^{2+}-free form of *E*2P produced from P_i without Ca^{2+} was as rapid in the mutants as in the wild type. Analysis of resistance against trypsin and proteinase K revealed that the structure of *E*2PCa_2 accumulated is an intermediate state between the *E*1PCa_2 and Ca^{2+}-released *E*2P states. Namely, in *E*2PCa_2, the Actuator domain is already largely rotated from its position in *E*1PCa_2 and associated with the Phosphorylation domain as in the Ca^{2+}-released *E*2P state, however in *E*2PCa_2 the hydrophobic interactions among these domains and Leu^{119}/Tyr^{122} on the top of 2nd transmembrane helix is not formed properly yet. This is consistent with our previous finding that these interactions at Tyr^{122} are critical for formation of Ca^{2+}-released *E*2P structure. Results showed that the *E*P isomerization/Ca^{2+}-release process consists of two steps; *E*1PCa_2 → *E*2PCa_2 → *E*2P + 2Ca^{2+}, and the intermediate state *E*2PCa_2 was identified for the first time. Results further indicated that the A/M1-linker with its appropriately short length, probably because of the strain imposed in *E*2PCa_2, is critical for the correct positioning and interactions of the Actuator and Phosphorylation domains to cause structural changes for the Ca^{2+} deocclusion and release.

Sarcoplasmic reticulum Ca^{2+}-ATPase (SERCA1a)[2] is a representative member of P-type ion transporting ATPases and catalyzes Ca^{2+} transport coupled with ATP hydrolysis (Fig. 1) (Refs. 1 and 2, and for recent reviews, see Refs. 3-7). In the catalytic cycle, the enzyme is activated by binding of two Ca^{2+} ions to the transport sites (*E*2 to *E*1Ca_2, steps 1-2) and then autophosphorylated at Asp^{351} with MgATP to form the ADP-sensitive phosphoenzyme (*E*1P, step 3), which can react with ADP to regenerate ATP in the reverse reaction. Upon formation of this *E*P, the bound Ca^{2+} ions are occluded in the transport sites (*E*1PCa_2). The subsequent isomeric transition to the ADP-insensitive form (*E*2P), *i.e.* the loss of the ADP-sensitivity at the catalytic site, results in rearrangements of the Ca^{2+} binding sites to deocclude Ca^{2+}, reduce the affinity, and open the lumenal gate, thus release Ca^{2+} into lumen (steps 4-5). As an intermediate state in the *E*P isomerization/Ca^{2+}-release process, *E*2PCa_2 has been postulated (*e.g.* see Ref. 8) although this state has never been identified. Finally, the *E*2P hydrolysis takes place and returns the enzyme into an unphosphorylated and Ca^{2+}-unbound form (*E*2, steps 6-7). The transport cycle is totally reversible, *e.g.* *E*2P can be formed from P_i in the presence of Mg^{2+} and absence of Ca^{2+} by reversal of its hydrolysis, and the subsequent addition of high

concentrations of Ca^{2+} to *E*2P reverse the Ca^{2+}-releasing step and the *E*1P to *E*2P isomerization.

The enzyme has 3 cytoplasmic domains, Nucleotide-binding (N), Phosphorylation (P), and Actuator (A) domains, and 10 transmembrane helices M1-M10 (Fig. 2). During the *E*P isomerization/Ca^{2+}-release $E1PCa_2 \rightarrow E2P + 2Ca^{2+}$, the A domain largely rotates (by ~110°) parallel to membrane and associates with the P domain (Refs. 9-17, see $E1\cdot AlF_x\cdot ADP$ ($E1PCa_2\cdot ADP$ analog) → $E2\cdot MgF_4^{2-}$ ($E2\cdot P_i$ analog) in Fig. 2). The interactions of the A domain with the P domain in the *E*2P state occur at three regions (*semitransparent purple, blue,* and *orange* on $E2\cdot MgF_4^{2-}$); *i.e.* at the T^{181}GES loop with the residues of the P domain around Asp^{351}, at the Val^{200} loop (Asp^{196}-Asp^{203}) with the polar residues of the P domain (Arg^{678}/Glu^{680}/Arg^{656}/Asp^{660}), and at the Tyr^{122}-hydrophobic cluster formed by seven hydrophobic residues gathered from the A domain (Ile^{179}/Leu^{180}/Ile^{232}), the P domain (Val^{705}/Val^{726}), and the top part of M2 (the A/M2-linker region, Leu^{119}/Tyr^{122}). The formation of the A-P domain interaction at the T^{181}GES loop has been predicted to be critical for the loss of ADP-sensitivity at the catalytic site, *i.e.* the *E*1P to *E*2P isomerization, by the structural and mutation studies (18-20). The mutations at the latter two interaction regions were shown to not inhibit the *E*1P to *E*2P isomerization but markedly retard the subsequent *E*P decay (19, 21, 22). Its kinetics were consistent with the view that there is a Ca^{2+}-releasing step from $E2PCa_2$ ($E2PCa_2 \rightarrow E2P + 2Ca^{2+}$) before the *E*2P hydrolysis and that this Ca^{2+}-releasing step is blocked and became the kinetic limit for the *E*P decay by the disruption of the A-P domain interactions at each of the latter two regions (19, 21, 22). It is therefore very interesting to know how the motions and interactions of the A and P domains progress during the postulated successive steps $E1PCa_2 \rightarrow E2PCa_2 \rightarrow E2P + 2Ca^{2+}$ as the key structural events in the energy coupling between the cytoplasmic and transmembrane domains. In this respect, it is also critical to clarify and distinguish structural roles of the three linkers connecting the A domain with M1'/M1, M2, and M3 (A/M1-, A/M2-, and A/M3-linkers). Tyr^{122}/Leu^{119} involved in the aforementioned Tyr^{122}-hydrophobic cluster is at the A/M2-linker region. The A/M3-linker, because of its strain, has been predicted to be important for the large rotation of the A domain in the *E*P isomerization (12, 13).

Regarding the A/M1-linker, we recently found (23) that its shortening by deletions of any single residues within this linker (Glu^{40}-Ser^{48}) blocks the *E*1P to *E*2P isomerization and the hydrolysis of the Ca^{2+}-free form of *E*2P, whereas substitutions of any residues in this linker do not inhibit the function. Our results indicated that the A/M1-linker with its correct length critically contributes to the *E*P isomerization/Ca^{2+} release and to the *E*2P hydrolysis, and pointed out a possible importance of this linker in the proper positioning of the A and P domains for their motions and association during these processes. Therefore in the present study, we further explored the structural roles of this linker and structural events occurring in the processes by elongating this linker with insertion of glycines (see Fig. 2).

Results demonstrated that the elongation of the linker markedly accelerates the $E1PCa_2$ to $E2PCa_2$ isomerization, strongly stabilizes $E2PCa_2$ that possesses two occluded Ca^{2+} ions at the transport sites, and blocks the Ca^{2+} deocclusion and release from $E2PCa_2$. Thus, for the first time, the intermediate state $E2PCa_2$ was identified and trapped in this study. We were then able to characterize the structure of this state. Results revealed that the correct length of A/M1-linker is critical for structural events in each of successive steps in $E1PCa_2 \rightarrow E2PCa_2 \rightarrow E2P + 2Ca^{2+}$, and $E2P + H_2O \rightarrow E2 + P_i$, and further suggested how the motions and interactions of the properly positioned A and P domains progress with the critical contribution of the linker to accomplish the successive structural events in these steps. Our study also revealed an importance of M1' directly connected with the A/M1-linker likely for forming the base of this linker.

EXPERIMENTAL PROCEDURES

Mutagenesis and Expression — The Stratagene QuikChange™ site-directed mutagenesis method (Stratagene, La Jolla, CA) was utilized for the insertions and substitutions of residues in the rabbit SERCA1a cDNA. The *Apa*I-*Kpn*I restriction fragments with the desired mutation were excised from the plasmid and ligated back into the corresponding region in the full-length SERCA1a cDNA in the pMT2 expression vector (24). The pMT2 DNA was transfected into COS-1 cells by the liposome-mediated transfection method. Microsomes were prepared from the cells as described previously (25). The "control microsomes" were prepared from COS-1 cells transfected with the pMT2 vector containing no SERCA1a cDNA. The amount of expressed SERCA1a was quantified by a sandwich enzyme-linked immunosorbent assay as described previously (26). Expression levels of the wild-type SERCA1a and mutants examined in this study were 2-3% of total microsomal proteins, except a mutant 4950525354S for M1' with serine-substitutions of $Leu^{49}/Trp^{50}/Leu^{52}/Val^{53}/Ile^{54}$, which showed markedly reduced expression (only ~15-20% of the wild type).

Ca^{2+}-ATPase Activity — The rate of ATP hydrolysis was determined at 25 °C in a mixture containing 1 μg of microsomal protein, 0.1 mM [γ-^{32}P]ATP, 1 μM A23187, 0.1 M KCl, 7 mM $MgCl_2$, 0.55 mM $CaCl_2$, 0.5 mM EGTA, and 50 mM MOPS/Tris (pH 7.0). The Ca^{2+}-ATPase activity was obtained by subtracting the Ca^{2+}-independent ATPase activity, which was determined in the presence of 5 mM EGTA without added $CaCl_2$, otherwise as above. The ATPase activity/mg of expressed SERCA1a protein was calculated from the amount of expressed SERCA1a and the Ca^{2+}-ATPase activity of expressed SERCA1a, which was obtained by subtracting the Ca^{2+}-ATPase activity of the control microsomes from that of the microsomes expressing SERCA1a. This background level with the control microsomes was as low as 3% of the activity of microsomes expressing the wild-type SECRA1a.

Formation and Hydrolysis of EP — Phosphorylation of SERCA1a in microsomes with [γ-^{32}P]ATP or $^{32}P_i$, and dephosphorylation of ^{32}P-labeled SERCA1a were performed under conditions described in the legends to figures. The reactions were quenched with ice-cold trichloroacetic acid containing P_i. Rapid kinetics measurements of phosphorylation and dephosphorylation were performed with a handmade rapid mixing apparatus (27), otherwise as above. The precipitated proteins were separated by 5% SDS-PAGE at pH 6.0 according to Weber and Osborn (28). The radioactivity associated with the separated Ca^{2+}-ATPase was quantitated by digital autoradiography as described (29). The amount of *E*P formed with the expressed SERCA1a was obtained by subtracting the background radioactivity with the control microsomes. This background was less than 5% of the radioactivity of *E*P formed with the expressed wild-type SERCA1a. The amount of *E*P/mg of SERCA1a protein was calculated from the amount of *E*P thus obtained and the amount of expressed SERCA1a.

Ca^{2+} Occlusion in EP — As described in the legend for Fig. 8, the expressed mutant SERCA1a in microsomes was phosphorylated with ATP and $^{45}CaCl_2$ and then the mixture was diluted by a "washing solution" containing excess EGTA and immediately filtered through a 0.45-μm nitrocellulose membrane filter (Millipore). The filter was washed 4 times with 2 ml of the washing solution, and $^{45}Ca^{2+}$ remaining on the filter was quantitated. The amount of Ca^{2+} specifically bound to the transport sites of *E*P in the expressed SERCA1a was obtained by subtracting the amount of nonspecific Ca^{2+}-binding, which was determined by including 1 μM thapsigargin (TG) in the phosphorylation mixture, otherwise as above. This background subtraction is assured by the fact that TG inhibits the Ca^{2+} binding at the transport sites and the *E*P formation (30). The background level thus determined was approximately 60% of the total amount of $^{45}Ca^{2+}$ remained on the filter when the maximum amount of *E*P was present (*i.e.* at the zero time of *E*P decay in Fig. 8). It should

be noted that the specifically bound Ca^{2+} in *E*P thus determined represents the occluded one because it is not released even after the extensive washing by EGTA. The Ca^{2+} occluded/mg of expressed SERCA1a protein was calculated from the amount of expressed SERCA1a and the amount of occluded Ca^{2+}. The Ca^{2+} occlusion resulted from Ca^{2+} binding to *E*2P in the reverse reaction of the Ca^{2+}-release process was also determined. In this case, *E*2P was first formed from P_i in the absence of Ca^{2+} and then $^{45}Ca^{2+}$ was added to *E*2P otherwise as described in the legend for Fig. 10, and the amount of occluded $^{45}Ca^{2+}$ was determined as above.

Limited Proteolysis of Major Intermediates and Western Blot Analysis — Major intermediates and its stable analogs of the Ca^{2+}-ATPase were produced and subjected to the structural analysis by limited proteolysis with trypsin and proteinase K (PrtK) as described in the legend to Fig. 12. The digests were separated by 10.5 or 7.5% SDS-PAGE according to Laemmli (31), and blotted onto a polyvinylidene fluoride membrane and then incubated with IIH11 monoclonal antibody to the rabbit SERCA1a (Affinity Bioreagents), which recognizes an epitope between Ala^{199}-Arg^{505}. After incubation with secondary antibody (goat anti-mouse IgG-horseradish peroxidase-conjugated), the bound proteins were probed using an enhanced chemiluminescence-linked detection system (ECL Plus, GE Healthcare Life Sciences).

Miscellaneous — Protein concentrations were determined by the method of Lowry *et al*. (32) with bovine serum albumin as a standard. Data were analyzed by nonlinear regression using the program Origin (Microcal Software, Inc., Northampton, MA). Three-dimensional models of the enzyme were reproduced by the program VMD (33).

RESULTS

Ca^{2+}-ATPase Activity — The specific Ca^{2+}-ATPase activity of the expressed SERCA1a mutants was determined at saturating 50 μM Ca^{2+} and 25 °C, and compared with that of the wild type (Fig. 3). Insertion of one glycine between Gly^{46} and Lys^{47} (1Gi-46/47) and between Pro^{42} and Ala^{43} (1Gi-42/43) within the A/M1-linker slowed the ATPase activity by ~50%. Insertion of two or more glycines at each of these sites abolished the activity almost completely (2Gi-46/47~6Gi-46/47 and 4Gi-42/43). Thus, the elongation of the linker by the glycines-insertion at the two different positions within the A/M1-linker exhibited the same inhibitory effects on the ATPase, indicating the importance of the correct length of this loop in the function [3].

We then examined possible effects of the four amino acids-insertion in the C- and N-terminal regions of the A/M1-linker; between Val^{53} and Ile^{54} on the helix M1' and between Thr^{22} and Gly^{23} in the immediate vicinity of the Thr^{25}-Tyr^{36} helix (see Fig. 2*b*). In these mutants 4Ai-53/54 and 4Ai-22/23, alanines were inserted (for M1', we intended to minimize possible disruption of the helical structure). These mutants exhibited the high ATPase activity (Fig. 3) and the Ca^{2+} transport coupled with the ATP hydrolysis (data not shown). Thus the insertions at the adjacent regions of the A/M1-linker did not inhibit the activity. We inserted amino acids also in the immediate N-terminal region of the A/M1-linker, for example at His^{32}-Leu^{33} and at Gly^{37}-His^{38}, however the protein expression levels of these mutants were extremely low (less than ~10% of the wild type) and therefore their functional analysis was not possible.

We also investigated possible importance of amphipathic property of the helix M1' (Trp^{50}-Glu^{58} in *E*1·AlF_x·ADP or Leu^{49}-Gln^{56} in *E*2·MgF_4^{2-}), which is directly connected with the A/M1-linker and formed by kinking of M1. M1' lies on the membrane surface, having hydrophobic residues aligned on the membrane side (Leu^{49}/Trp^{50}/Val^{53}/Ile^{54}) and the polar residues (Glu^{51}/Glu^{55}/Gln^{56}/Glu^{58}) on the cytoplasmic side (Fig. 2*b*). Therefore the hydrophobic interactions of M1' with the membrane core and/or its hydrophilic interactions at the membrane surface may possibly be important for function (13). Previously the mutations of the single residues

on the M1' region were found to have almost no or only slight effect on the activity (23, 34). In the present study, we therefore introduced the extensive non-conservative substitutions; the serine-substitution of all $Leu^{49}/Trp^{50}/Leu^{52}/Val^{53}/Ile^{54}$ (4950525354S) and the alanine-substitution of all $Glu^{51}/Glu^{55}/Gln^{56}/Glu^{58}/Asp^{59}$ (5155565859A). The mutant 4950525354S exhibited the markedly reduced ATPase activity (17% of that of the wild type), whereas the mutant 5155565859A a fairly high activity (70% of that of the wild type). The results indicate that the hydrophobic interaction of M1' with the membrane core may be important.

EP Formation from ATP and the E2-E1Ca$_2$ Transition — The amount of *E*P formed from ATP at saturating 50 μM Ca^{2+} was determined at steady state and 0 °C with 10 μM ATP under the conditions otherwise the same as those for the ATPase assay (*open bars* in Fig. 4). All the mutants formed *E*P with the amounts comparable to that of the wild type (3.31 ± 0.14 nmol/mg of the SERCA1a protein (n = 4)) except that the mutant 4950525354S exhibited somewhat reduced amount. The Ca^{2+} affinity of the mutants in the *E*2 to *E*1Ca_2 transition was estimated by the Ca^{2+}-dependence of the *E*P formation from ATP, and found to be nearly the same as that of the wild type (see the Ca^{2+} affinity and the Hill coefficient in Table I). The mutant 4Ai-53/54 among examined showed a slightly reduced affinity. We further found that the first order rate constants of the *E*2 to *E*1Ca_2 transition (steps 1-2) in the examined mutants were nearly the same as that in the wild type (Table I). In this experiment, the enzyme was first preincubated in the absence of Ca^{2+} at pH 6, where the equilibrium between *E*1 and *E*2 is most shifted to *E*2 (35), and then the phosphorylation was initiated by the simultaneous addition of saturating Ca^{2+} and ATP. When ATP was added to the enzyme preincubated with Ca^{2+} otherwise as above, the *E*P formation was much faster in the mutants as well as in the wild type, therefore the rates obtained above actually reflect the rate-limiting *E*2 to *E*1Ca_2 transition.

Loss of ADP-sensitivity in EP — The *E*1P to *E*2P isomerization, *i.e.* the loss of the ADP-sensitivity at the catalytic site, was analyzed at 0 °C under the conditions otherwise the same as those for the ATPase assay. In Fig. 4 (*closed bars*), the amount of ADP-insensitive *E*P (*E*2P) accumulated in the steady state was determined at 60 s after the addition of ATP in the presence of K^+, which strongly accelerates the hydrolysis of *E*2P and thus suppresses its accumulation in the wild type (36). In the mutants 1Gi-46/47 and 1Gi-42/43, the amount of the accumulated ADP-insensitive *E*P was very low as in the wild type, and it was markedly increased in the mutants with two or more glycines-insertion in the A/M1-linker, 2Gi-46/47~6Gi-46/47 and 4Gi-42/43 (compare with the total amount of *E*P shown by *open bar*). In the mutants with the three or more glycines-insertion, nearly all of *E*P was ADP-insensitive. The mutant 4950525354S for M1' also accumulated the ADP-insensitive *E*P almost exclusively. On the other hand, in the mutants 5155565859A for M1' and 4Ai-22/23 and 4Ai-53/54 for the adjacent regions of the A/M1-linker, the accumulation of ADP-insensitive *E*P was very low as in the wild type.

The observed markedly enhanced accumulation of ADP-insensitive *E*P in the mutants suggests that the *E*1P to *E*2P isomerization was accelerated and/or that the rate of one of the reverse transitions, *e.g.* from *E*2PCa_2 to *E*1PCa_2, was dramatically reduced. It is also possible that the decay of ADP-insensitive *E*P was blocked. In Fig. 5*A* and *B*, the time course of accumulation of ADP-insensitive *E*P from *E*1Ca_2 and ATP was determined in the absence of K^+, in which the wild type accumulates a fair amount of ADP-insensitive *E*P and thus the kinetics can be compared. The phosphorylation from *E*1Ca_2, *i.e.* the formation of ADP-sensitive *E*P (*E*1P) from *E*1Ca_2, occurred very rapidly and thus the total amount of *E*P reached its maximum level within a few seconds except for the slowed mutant 4950525354S (Fig. 5*A*). The accumulation of ADP-insensitive *E*P apparently proceeded with first order kinetics. The rate and extent of the accumulation in the mutants 1Gi-46/47, 2Gi-46/47 (Fig. 5*B*), and

1Gi-42/43 (data not shown) in the absence of K^+ were comparable to those of the wild type (see Table I for the rates). The accumulation of ADP-insensitive *E*P became extremely rapid in the mutants with three or more glycines-insertion, 3Gi-46/47 and 4Gi-46/47. Actually during the time course of *E*P formation in these mutants, nearly all of *E*P formed was already ADP-insensitive. Essentially the same results were obtained with the mutant 4Gi-42/43 as with these mutants (data not shown, but see Table I). Thus in the mutants with the elongated A/M1-linker with the three or more glycines-insertion, the *E*P isomerization was markedly accelerated and the ADP-insensitive *E*P (*E*2P) accumulated exclusively. In these mutants, the rates of *E*P formation and the *E*P isomerization in the presence of K^+ (Fig. 5*C*, *D*) were almost the same as those in the absence of K^+ (Fig. 5*A*, *B*). In the mutant 2Gi-46/47, the fair amount of ADP-insensitive *E*P accumulated rapidly even in the presence of K^+ (see Figs. 5*D* and 4).

It should be noted that the mutant 4950525354S exhibited the almost exclusive accumulation of ADP-insensitive *E*P both in the absence (Fig. 5*B*) and presence (Fig. 4) of K^+ at steady state. In this regard, the removal of the hydrophobic property of M1' by the serine-substitutions (removal of the likely hydrophobic interaction with the membrane core) caused the same consequence as that of the elongation of the A/M1-linker. Besides, the observed slow *E*P formation from $E1Ca_2$ and ATP in this mutant 4950525354S (Fig. 5*A*) suggests the importance of the hydrophobic property of this region in rapid structural changes for ATP-binding and phosphorylation. The mutants 5155565859A on M1' and 4Ai-22/23 and 4Ai-53/54 adjacent to the A/M1-linker exhibited the extent and rate of the accumulation of ADP-insensitive *E*P almost the same as those of the wild type (see Table I for the rates, and Figs. 5*B* and 4 for the extents).

Decay of EP Formed from ATP and Ca^{2+} — The decay of *E*P formed from ATP and Ca^{2+} was determined at 0 °C in the presence of K^+ and shown with the representative mutants in Fig. 6. The decay time courses were fitted well with a single exponential (Fig. 6*A*) and the rates were summarized in Table I. The fraction of the ADP-insensitive *E*P (*E*2P) remaining in the decay course was also determined (Fig. 6*B*). In the wild type, *E*P remaining was exclusively the ADP-sensitive *E*P (*E*1P), and this is consistent with the well-known rate-limiting *E*1P to *E*2P transition in the ATPase cycle (36, 37). The *E*P decay was slightly slowed in the single glycine-insertion mutants 1Gi-46/47 (Fig. 6*A*) and 1Gi-42/43 (see Table I), being consistent with the slight reduction in the ATPase activity in these mutants (*cf.* Fig. 3). The *E*P decay was almost completely blocked in the mutants with two or more glycines-insertion in the A/M1-linker, 2Gi-46/47~4Gi-46/47 (Fig. 6*A*) and 4Gi-42/43 (see Table I). This is consistent with the complete loss of the ATPase activity in these mutants. *E*P present at the start and course of the decay reaction was exclusively the ADP-insensitive one (*E*2P) in the mutants 3Gi-46/47 and 4Gi-46/47, and ~50% in the mutant 2Gi-46/47 (Fig. 6*B*, as also shown in Figs. 4 and 5*D*). These results show that, in the mutants with the elongated A/M1-linker with the two or more glycines-insertion, the *E*1P-*E*2P isomerization was strongly shifted toward the ADP-insensitive *E*P (*E*2P) and that the decay of the ADP-insensitive *E*P was blocked. In the mutant 4950525354S on M1', the *E*P decay was markedly slowed (Fig. 6*A*) and the *E*P remaining was almost exclusively the ADP-insensitive *E*P during the decay reaction (data not shown, but see Fig. 4). Thus in this mutant, the decay of the ADP-insensitive *E*P was markedly retarded. The mutants 5155565859A (Fig. 6*A*), 4Ai-22/23, and 4Ai-53/54 (Table I) showed the rapid *E*P decay as the wild type, being consistent with their high ATPase activities.

Hydrolysis of E2P Formed from P_i without Ca^{2+} — The observed block of decay of the ADP-insensitive *E*P (*E*2P) formed from ATP and Ca^{2+} in the mutants with the elongated A/M1-linker and 4950525354S might possibly be due to the block of hydrolysis of the Ca^{2+}-free form of *E*2P. Therefore, in Fig. 7, the *E*2P hydrolysis was directly examined by

first phosphorylating the enzyme with $^{32}P_i$ in the absence of Ca^{2+} and K^+ and presence of 35% (v/v) Me_2SO, which extremely favors the *E*2P formation in the reverse reaction (38), and then by diluting the phosphorylated sample at 0 °C with a large volume of solution containing non-radioactive P_i and K^+ without Ca^{2+}. The conditions for the hydrolysis were thus made otherwise the same as those for the decay of *E*P formed from ATP with Ca^{2+} in Fig. 6. Hydrolysis of ^{32}P-labeled *E*2P proceeded with first-order kinetics as shown with the representative mutants, and the rates obtained were summarized in Table I. To our surprise, in all the mutants with the elongated A/M1-linker 1Gi-46/47~6Gi-46/47, 1Gi-42/43, and 4Gi-42/43, the hydrolysis of *E*2P without bound Ca^{2+} occurred as rapidly as in the wild type. The mutants 4950525354S, 5155565859A, 4Ai-22/23, and 4Ai-53/54 also exhibited the rapid *E*2P hydrolysis as the wild type.

Ca^{2+} Occlusion in Stable E2P — The observed block of the decay of ADP-insensitive *E*P (*E*2P) formed from ATP with Ca^{2+} (Fig. 6) and the rapid hydrolysis of *E*2P formed from P_i without Ca^{2+} (Fig. 7) in the mutants indicate that there may be a kinetic limit for the decay of *E*2P formed with Ca^{2+} before the hydrolysis of *E*2P without bound Ca^{2+}. This limiting step is possibly the Ca^{2+}-releasing step from *E*2PCa_2; *E*2PCa_2 → *E*2P + $2Ca^{2+}$, and *E*2PCa_2 may be stabilized and accumulated in the mutants. In Fig. 8, this possibility was directly examined by the determination of $^{45}Ca^{2+}$ occlusion in *E*2P accumulated from ATP and $^{45}Ca^{2+}$. With the representative mutants 4Gi-46/47 (Fig. 8*A*, *C*) and 2Gi-46/47 (Fig. 8*B*, *C*), *E*P was first formed from ATP and $^{45}Ca^{2+}$ at steady state in the absence or presence of the Ca^{2+}-ionophore A23187, and then the *E*P decay was initiated by the addition of excess EGTA. The amount of occluded $^{45}Ca^{2+}$ was determined at the indicated time by membrane filtration with an extensive washing with a solution containing EGTA and A23187. The total amount of *E*P and the fraction of ADP-insensitive *E*P (*E*2P) was determined by the use of [γ-^{32}P]ATP and non-radioactive Ca^{2+}.

The extremely slow *E*P decay was observed at 25 °C with the mutant 4Gi-46/47 (Fig. 8*A*). At the zero time of the decay reaction, the amount of occluded Ca^{2+} and that of *E*P were approximately 9 and 4~4.5 nmol/mg of expressed SERCA1a protein, respectively, both in the presence and absence of A23187. These values gave the stoichiometry "two occluded Ca^{2+} ions per one *E*P". The amount of $^{45}Ca^{2+}$ remaining on the membrane filter decreased concomitantly with the *E*P decay, and therefore the stoichiometry was always found to be "two" during the *E*P decay course (Fig. 8*C*). This stoichiometry is in complete agreement with the presence of two Ca^{2+} binding (transport) sites in the ATPase molecule. Importantly, *E*P remaining during the decay-time course was exclusively the ADP-insensitive one (*E*2P) in this mutant 4Gi-46/47 (data not shown, but see Fig. 6*B*). Thus, the results clearly demonstrated that *E*P accumulated in the mutant is the ADP-insensitive *E*P that possesses two occluded Ca^{2+} ions, *i.e.* *E*2PCa_2, and the Ca^{2+} deocclusion from *E*2PCa_2 is extremely slowed by the elongation of the A/M1-linker and therefore *E*2PCa_2 is accumulated exclusively. The decay of *E*2PCa_2 became faster by A23187 (although only slightly), being consistent with the mechanism that the Ca^{2+} release occurs into lumen from *E*2PCa_2. It should be noted that this type of experiments was not possible with the wild type because its *E*P decay is extremely rapid and completed during the EGTA washing (actually within 1 s).

In Fig. 8*B* and *C*, the experiments were performed with the mutant 2Gi-46/47 in the presence of A23187 at 10 °C. At this temperature, the *E*P decay was most conveniently followed in this mutant. The phosphorylated samples were filtered at the indicated time with and without addition of ADP immediately before the filtration. Approximately 50% of the total amount of *E*P was ADP-insensitive *E*P (*E*2P) throughout the decay reaction (compare *open* and *closed squares* in Fig. 8*B*, also see Fig. 6*B*). The total amount of *E*P, the amount of ADP-insensitive *E*P, and the amounts of occluded Ca^{2+} determined without and with the

ADP addition decreased very slowly and concomitantly (Fig. 8*B*). Thus as plotted in Fig. 8*C*, the stoichiometry of the occluded Ca^{2+} was always found to be "two" in the total amount of *E*P (*E*1P plus *E*2P) and in the amount of ADP-insensitive *E*P (*E*2P) throughout the decay reaction. The results show that two Ca^{2+} ions are occluded in both the ADP-sensitive *E*P, *i.e.* *E*1PCa_2, and the ADP-insensitive *E*P, *i.e.* *E*2PCa_2, in the mutant 2Gi-46/47. The results are consistent with the view that the *E*1PCa_2-*E*2PCa_2 equilibrium was largely shifted to *E*2PCa_2 and the Ca^{2+} deocclusion from *E*2PCa_2 was blocked in this mutant. It should be mentioned for the mutant 4950525354S that, as indicated by the kinetic analyses in Figs. 4-7, *E*2PCa_2 is probably accumulated in this mutant from ATP and Ca^{2+} as in the mutant 4Gi-46/47. The Ca^{2+} binding experiments were however not possible with this mutant because of its very low protein-expression level (only ~15-20 % of that of 4Gi-46/47 and 2Gi-46/47 or wild type).

Formation of Stable E2PCa_2 from E2P and Ca^{2+} in Reverse Reaction — As demonstrated with SR Ca^{2+}-ATPase (39), the *E*1P to *E*2P transition and the Ca^{2+} release into lumen can be reversed by the low-affinity Ca^{2+} binding from the lumenal side to the transport sites of the Ca^{2+}-free form of *E*2P. In Fig. 9, we examined with the representative mutants whether the stable *E*2PCa_2 can be produced in the reverse reaction. In the experiments, *E*2P was first formed from $^{32}P_i$ without Ca^{2+} in the presence of A23187 and 35% (v/v) Me_2SO that strongly favors *E*2P (38), and subsequently the phosphorylation mixture was diluted 10-fold with a solution containing $CaCl_2$ to give a very high (saturating) Ca^{2+} concentration of 20 mM. After one minute incubation with Ca^{2+}, the mixture was further diluted 10-fold with a solution containing excess EGTA and 0.1 M KCl, and the decay of *E*P was followed at 0 °C. Thus, the final conditions for this *E*P decay in Fig. 9 were made to be essentially the same as those for the decay of *E*P formed from ATP and Ca^{2+} in the forward reaction in Fig. 6. We observed actually the same time courses in Fig. 9 as those in Fig. 6 for each of the representative mutants as well as for the wild type. Most importantly, in the mutants with the two or more glycines-insertion in the A/M1-linker (2Gi-46/47, 3Gi-46/47, and 4Gi-46/47), the decay of *E*P formed from *E*2P with the subsequently added Ca^{2+} was nearly completely blocked. Furthermore, *E*P remaining during the decay course was exclusively the ADP-insensitive one in the mutants 3Gi-46/47 and 4Gi-46/47, and ~50% in the mutant 2Gi-46/47 (Fig. 9*B*). The results show that the stable *E*2P, probably *E*2PCa_2, is formed in these mutants in the reverse reaction from *E*2P and Ca^{2+} as well as in the forward reaction with ATP and Ca^{2+}. In the wild type, *E*2P formed from P_i became exclusively the ADP-sensitive one (*E*1PCa_2) upon the Ca^{2+} addition, being consistent with the previous observation (39).

With the representative mutant 4Gi-46/47, we then actually determined the $^{45}Ca^{2+}$ occlusion in the stable *E*2P formed from *E*2P with the subsequently added 3 mM $^{45}Ca^{2+}$ (rather than 20 mM because of the experimental limitation) otherwise as above [4]. We found that the amounts of stable *E*2P formed and the occluded Ca^{2+} were 1.65 ± 0.13 and 3.33 ± 0.25 nmol/mg of expressed SERCA1a protein (n = 4), respectively, thus the stoichiometry of the occluded Ca^{2+} in *E*2P was 2.02. The results demonstrated that two Ca^{2+} ions are occluded in the stable *E*2PCa_2, which is formed in the reverse reaction as in the forward reaction. The results also indicated that the reverse transition from *E*2PCa_2 to *E*1PCa_2 is dramatically retarded (blocked) in the mutants 3Gi-46/47 and 4Gi-46/47.

Accessibility of Lumenal Ca^{2+} to Transport Sites of E2P Formed from P_i — We then measured the Ca^{2+} concentration dependence of the Ca^{2+}-induced formation of the stable *E*P from *E*2P and Ca^{2+} in the reverse reaction (Fig. 10). In the experiments, *E*2P was first formed from P_i without Ca^{2+} in the presence of A23187, and subsequently the phosphorylation mixture was largely diluted with a solution containing $CaCl_2$ to give the free Ca^{2+} concentrations indicated in Fig. 10. Immediately after this Ca^{2+} addition, the *E*P decay was followed without removing Ca^{2+}. As typically shown in Fig. 10*A* and *B* for the

wild type and the mutant 2Gi-46/47, the decay of *E*P proceeded with two phases as previously shown in this type of experiments with the Ca^{2+}-ATPase (40). The first and rapid phase corresponds to the hydrolysis of *E*2P without bound Ca^{2+}. In the wild type, the second and very slow phase corresponds to the forward decay of *E*1PCa_2 that is formed from *E*2P and Ca^{2+}, as well documented previously (39, 40). In fact, nearly all the *E*P remaining in the decay course was the ADP-sensitive one (*E*1P) in the wild type (data not shown).

In the mutants 2Gi-46/47 (Fig. 10*B*) and 3Gi-46/47 and 4Gi-46/47 (data not shown), the *E*P decay in the second phase was extremely slow and actually almost no decay occurred during the period of observation. The decay of *E*P in these mutants was extremely slow even after removal of Ca^{2+} as shown in Fig. 9. *E*P remaining in this slow phase was almost exclusively the ADP-insensitive one (*E*2P) in the mutants 3Gi-46/47 and 4Gi-46/47 even at the highest Ca^{2+} concentration 20 mM and approximately 50% in the mutant 2Gi-46/47 at 20 mM Ca^{2+} (see Fig. 9).

The content of *E*P in the second and slow phase was obtained by extrapolating to the zero time and plotted *versus* the Ca^{2+} concentrations (Fig. 10*C*). The content increased with the increase in the Ca^{2+} concentration and was nearly saturated at ~10 mM Ca^{2+}. $K_{0.5}$ was estimated to be 1.4 mM in the wild type and similarly 0.9-1.3 mM in the mutants in Fig. 10, and other mutants as well (see Table I). These values are actually consistent with the high Ca^{2+} concentrations required for the Ca^{2+}-induced reverse reaction from *E*2P previously determined with SR Ca^{2+}-ATPase as the access of lumenal Ca^{2+} to the transport sites of *E*2P (41-44). The results indicate that in these mutants with the elongated A/M1-linker, the lumenal Ca^{2+} can access and bind to the transport sites of *E*2P as in the wild type, and the mutants produce the stable ADP-insensitive *E*P, *i.e.* *E*2PCa_2.

In this context, it should be noted that the Ca^{2+}-dependent increase in the stable *E*P in Fig. 10*C* reflects mostly the relative values between the Ca^{2+}-dependently increasing rate of the formation of the stable *E*P *versus* the rate of the hydrolysis of the Ca^{2+}-unbound *E*2P. Namely, the curve reflects mostly the relative rates between [*E*2P + 2Ca^{2+} → *E*2PCa_2 (or further to *E*1PCa_2)] *versus* [*E*2P + H_2O → *E*2 + P_i], rather than the relative rates between the reverse and forward reactions in [*E*2P + 2Ca^{2+} ↔ *E*2PCa_2 (or *E*1PCa_2)] (*i.e.* the Ca^{2+} affinity). This is because the curve in Fig. 10*C* is the plot of the amount of *E*P stably remaining after the hydrolysis of the Ca^{2+}-unbound *E*2P, and because the amount of the remaining *E*P is dependent on the rate of its formation relative to the rate of the *E*2P hydrolysis. Furthermore, the decay of the remaining *E*P in the second phase was extremely slow in the wild type as well as in the mutants, and thus virtually negligible as compared with its rapid formation and the rapid hydrolysis of the Ca^{2+}-unbound *E*2P both in the wild type and mutants (see footnote 5). Importantly, the *E*2P hydrolysis rate was found to be essentially the same between the wild type and the mutants (Fig. 7). Therefore, the very similar Ca^{2+}-dependence curves of the wild type and mutants in Fig. 10*C* indicate that the rates of the formation of the stable *E*P upon the lumenal Ca^{2+}-binding to *E*2P are very similar between them. Thus we concluded that *E*2P formed from P_i without Ca^{2+} in the mutants possesses the lumenally opened Ca^{2+} release pathway as in the wild type.

Decomposition of Stable E2PCa₂ by Thapsigargin — Thapsigargin (TG) is well known to bind very tightly to a specific site on the transmembrane helices of the Ca^{2+}-free *E*2 form of SERCA, and fix their orientation to produce a very stable complex *E*2(TG) (10, 30, 45, 46). In addition, it was previously suggested by the P_i ↔ HOH oxygen exchange (47) that TG stimulates the dephosphorylation (the acylphosphate hydrolysis reaction step) of the Ca^{2+}-unbound form of *E*2P (especially in the presence of Me_2SO). In Fig. 11, we examined a possible effect of TG on *E*2PCa_2 exclusively accumulated with the representative mutant 4Gi-46/47. *E*2PCa_2 was first formed in the forward reaction from ATP and Ca^{2+} as in Fig. 6*A*, and also in the reverse reaction from P_i with the subsequently added 20 mM Ca^{2+} as in Fig. 9*A*. Then excess

EGTA was added with or without TG, and the dephosphorylation was followed at 25 °C. The results demonstrated that TG accelerates the dephosphorylation of $E2PCa_2$ in both cases strongly and equally, and therefore $E2PCa_2$ accumulated is sensitive to TG. It is very likely that TG binds to $E2PCa_2$ and its binding accelerates the Ca^{2+} deocclusion and release from $E2PCa_2$. This is because $E2PCa_2$ is the exclusively accumulated one and there is no $E2P$ and no $E2$ (that are known to bind TG), and because the decay of $E2PCa_2$ in the presence of TG took place with the rate 0.01 s^{-1} (Fig. 11) and this is still far slower than the hydrolysis of the Ca^{2+}-released form of $E2P$. Actually the $E2P$ hydrolysis of the mutants as well as of the wild type was completed within 1 sec at 25 °C under the conditions in Fig. 11 in the absence and presence of TG (data not shown). Consistently, the rate of the $E2P$ hydrolysis was previously reported with SR Ca^{2+}-ATPase to be 60~120 s^{-1} in the absence or presence of TG (42, 47) at this temperature (25 °C) under very similar conditions. Thus the effect of TG on the decomposition of $E2PCa_2$ is shown here for the first time.

Structure of $E2PCa_2$ Revealed by Proteolytic Analysis As an Intermediate State between $E1PCa_2$ and $E2P$ — In the transport cycle, the cytoplasmic three domains, N, P, and A largely move and change their organization states (7, 9-17). These changes are definitely monitored as the changes in the resistance of the specific cleavage sites against trypsin and proteinase K (PrtK) (15-17). As one of most notable example, the tryptic T2 site Arg^{198} on the outermost Val^{200} loop (Asp^{196}-Asp^{203}) of the A domain is rapidly cleaved in $E1PCa_2$, by contrast, it is completely resistant in $E2P$ (15-17). This is because the A domain largely rotates parallel to the membrane plane by ~110°, and the Val^{200} loop including Arg^{198} associates with the P domain by forming an ionic interaction network and thus blocks sterically against the tryptic attack, as seen in $E1\cdot AlF_x\cdot ADP \rightarrow E2\cdot MgF_4^{2-}$ (or $E2\cdot AlF_4^-$) (11-14, see Figs. 2 and 13).

In the *upper panel* of Fig. 12*A*, the trypsin proteolysis was performed with the wild type for the major intermediates and their structural analogs stabilized by the appropriate ligands according to the previous findings (15-17). The ATPase chain and its fragments were immunodetected with a monoclonal antibody that recognizes Ala^{199}-Arg^{505} (the tryptic fragment "A1") of SERCA1a. In all the structural states, the T1 site (Arg^{505}) on the outermost loop of the N domain was very rapidly cleaved to produce the fragment "A" (Met^1 to Arg^{505}, as immunodetected) and the fragment "B" (Ala^{506} to the C-terminus Gly^{994}, not immuno-monitored). In the structural states $E2$, $E1Ca_2$, $E1\cdot AlF_x\cdot ADP$ ($E1PCa_2\cdot ADP$ analog), and $E1PCa_2$ accumulated exclusively with the wild type from ATP at a very high concentration (5 mM) of Ca^{2+}, the T2 site was rapidly cleaved to produce the fragment "A1" as immunodetected and the fragment "A2" (Met^1-Arg^{198}, not immuno-monitored). By contrast, in the structural states of $E2P$ without bound Ca^{2+} stabilized by orthovanadate ($E2V_i$) and by Al^{3+}/F^- ($E2\cdot AlF_4^-$, the transition state analog of the $E2P$ hydrolysis (17)), the T2 site was completely resistant. The complete resistance was also found with $E2\cdot MgF_4^{2-}$ and $E2\cdot BeF_x$, the $E2\cdot P_i$ analog and the $E2P$ ground state analog respectively (17) (data not shown). These results with the wild type agree with the previous demonstration with SR Ca^{2+}-ATPase (15-17).

In the lower panel of Fig. 12*A* for the representative mutant 4Gi-46/47, the distinct finding was obtained with EP accumulated from ATP and Ca^{2+}, which was exclusively $E2PCa_2$ as demonstrated in Figs. 6 and 8. In $E2PCa_2$, the T2 site was completely resistant to tryptic attack as clearly shown by the exclusive accumulation of the fragment "A" without any further cleavage (*i.e.* without any formation of "A1"). This is in sharp contrast to its rapid cleavage in $E1PCa_2$ accumulated from ATP with the wild type and in the $E1PCa_2$ structural state of the mutant and wild type stabilized as $E1\cdot AlF_x\cdot ADP$. In the Ca^{2+}-unbound $E2P$ structural analogs ($E2V_i$, $E2\cdot AlF_4^-$, $E2\cdot MgF_4^{2-}$, and $E2\cdot BeF_x$), the T2 site in the mutant was completely resistant as in the wild type. The results show that, in $E2PCa_2$ accumulated with the mutant, the A domain is already largely rotated from its position in $E1PCa_2$ and

associated with the P domain at the T2 site region (Val^{200} loop) as in the Ca^{2+}-unbound *E*2P state. This agrees with the fact that *E*2PCa_2 accumulated is ADP-insensitive, because the loss of the ADP-sensitivity is brought about by the association of the largely rotated A domain with the P domain (13-17, 21, see Figs. 2 and 13).

In Fig. 12*B*, the same set of experiments was performed with PrtK. As previously demonstrated with SR Ca^{2+}-ATPase (48, 49), in the *E*2 state, PrtK cleaved at Leu^{119} on the top part of M2 (A/M2-linker region, see Figs. 2 and 13) producing the fragment "p95", and more slowly at Thr^{242} on the A/M3-linker and Ala^{746} on M5 producing the fragments "p81/83". The Leu^{119}-site became resistant in *E*1Ca_2, and all the sites were nearly completely resistant in *E*1PCa_2 accumulated from ATP with the wild type and in the *E*1PCa_2 structural state (*E*1·AlF_x·ADP) produced with the wild type and with the mutant. The ATPase chain was also completely resistant in the Ca^{2+}-unbound *E*2P structural analogs *E*2V_i, *E*2·AlF_4^- (Fig. 12*B*), *E*2·MgF_4^{2-}, and *E*2·BeF_x, (data not shown). These observations in the wild type and the mutant are in complete agreement with the previous demonstration with SR Ca^{2+}-ATPase (15-17). Distinct finding was obtained with *E*2PCa_2 accumulated with the mutant. Namely, a fairly rapid cleavage at Leu^{119} occurred in *E*2PCa_2 to produce "p95", being in sharp contrast to its resistance in the *E*1PCa_2 state and the Ca^{2+}-unbound *E*2P state. The results show that the structure at Leu^{119} in *E*2PCa_2 differs distinctly from those in *E*1PCa_2 and in the Ca^{2+}-free form of *E*2P.

In this regard, it is essential to note the fact that the structural bases rendering the complete resistance at Leu^{119} are totally different between *E*1PCa_2 and the Ca^{2+}-free form of *E*2P, as clearly seen in the structures *E*1·AlF_x·ADP and *E*2·MgF_4^{2-} (see Fig. 13). The resistance in *E*1PCa_2 (*E*1·AlF_x·ADP) is most likely due to the steric blocking against PrtK brought about by van der Waals contacts of the top part of M2 including Leu^{119} with the top part of M4 (Asn^{330}/Ile^{332}). On the other hand, in the Ca^{2+}-free form of *E*2P (*E*2·MgF_4^{2-} and *E*2·AlF_4^-), the resistance is most likely due to the steric blocking brought about by van der Waals contacts of Leu^{119} with the hydrophobic residues in the interaction network "Tyr^{122}-hydrophobic cluster" formed from the A and P domains and the top part of M2 (A/M2-linker region). This cluster actually consists of Ile^{179}/Leu^{180}/Ile^{232} at the bottom part of the A domain, Val^{705}/Val^{726} of the P domain, and Leu^{119}/Tyr^{122} at the top part of M2. Then a structural basis for the observed rapid cleavage at Leu^{119} in *E*2PCa_2, the intermediate state between *E*1PCa_2 and *E*2P, can be deduced from the structural change *E*1·AlF_x·ADP → *E*2·MgF_4^{2-} (or *E*2·AlF_4^-), which is the presently available model for the overall change in *E*1PCa_2 → *E*2P + $2Ca^{2+}$ (Fig. 13). During this change, the A domain largely rotates and M2 largely inclines away from its original position in *E*1PCa_2. Also the P domain inclines toward the bottom part of the A domain and associates with the A domain and top part of M2. Hence, the Leu^{119}-region on the top part of M2 widely separates from M4 and comes to Ile^{179}/Leu^{180}/Ile^{232} of the rotated A domain, and Val^{705}/Val^{726} of the P domain moves down to these residues to form the Tyr^{122}-hydrophobic cluster. It is therefore very likely that Leu^{119} will become sterically available to the PrtK-attack in the intermediate structural state during this change, especially if such state is trapped and stably accumulated. Such case was probably achieved in *E*2PCa_2 accumulated with the mutants with the elongated A/M1-linker. It is concluded that the Tyr^{122}-hydrophobic cluster is not formed properly yet in *E*2PCa_2 although in this state the A domain is already largely rotated and associated with the P domain at the Val^{200} loop (the T2 site region).

DISCUSSION

In this study, we explored the functional importance of the length of the A/M1-linker (Glu^{40}-Ser^{48} loop) and found that its elongation markedly accelerates the loss of the ADP-sensitivity in *E*P (the *E*1P to *E*2P isomerization) but blocks almost completely the decay of ADP-insensitive *E*P accumulated.

This *E*P was demonstrated to be *E*2PCa$_2$ having two occluded Ca^{2+} ions at the transport sites, and the Ca^{2+} deocclusion and release from *E*2PCa$_2$ was blocked. On the other hand, the hydrolysis of the Ca^{2+}-free form of *E*2P produced from the *E*2 state with P_i in the mutants was as rapid as in the wild type. The stable *E*2PCa$_2$ of the mutants was also produced in the reverse reaction upon addition of high concentrations of Ca^{2+} to *E*2P formed from P_i without Ca^{2+}, and the reverse isomerization from *E*2PCa$_2$ to *E*1PCa$_2$ was blocked in the mutants.

The results indicate that the *E*P isomerization/Ca^{2+}-release process described as a single step *E*1PCa$_2$ → *E*2P + 2Ca^{2+} consists of or can be dissected into the two successive steps; *E*1PCa$_2$ → *E*2PCa$_2$ → *E*2P + 2Ca^{2+}, *i.e.* the loss of ADP-sensitivity at the catalytic site (the *E*P isomerization) and the subsequent Ca^{2+}-release into lumen. This mechanism actually agrees with the one previously postulated on SR Ca^{2+}-ATPase although the intermediate state *E*2PCa$_2$ has never been identified and its mere presence has been questioned (*e.g.* Ref. 50, see footnote 6). In the present study, we could successfully trap and thus identify this *E*2PCa$_2$ state for the first time. *E*2PCa$_2$ accumulated was actually shown to possess the structural feature as the intermediate state between *E*1PCa$_2$ and the Ca^{2+}-released form of *E*2P (Fig. 12), and the results revealed the critical importance of the length of the A/M1-linker in the Ca^{2+} deocclusion and release from *E*2PCa$_2$.

Importantly, our previous study showed (23) that the substitutions of any residues in the A/M1-linker do not inhibit the reaction cycle, whereas the shortening of the linker by a deletion of any single residues in this linker almost completely blocks the *E*1PCa$_2$ to *E*2PCa$_2$ isomerization and the hydrolysis of the Ca^{2+}-free form of *E*2P. Thus, the length of this linker is obviously critical for each of the successive three steps; *E*1PCa$_2$ → *E*2PCa$_2$ → *E*2P + 2Ca^{2+} and *E*2P + H_2O → *E*2 + P_i, and the shortening and the elongation of the linker both cause the severe defects but in the distinct steps [7]. Based on the results and the crystal structures, we discussed below the structural roles of the A/M1-linker in each of the three steps and dissected the structural events occurring in these steps.

Loss of ADP-sensitivity; the E1PCa$_2$ to E2PCa$_2$ Isomerization — The loss of ADP-sensitivity at the catalytic site (the *E*P isomerization) involves the large rotation of the A domain approximately parallel to the membrane plane and its association with the P domain (see *E*1·AlF_x·ADP → *E*2·MgF_4^{2-} in Figs. 2 and 13). Thereby the outermost T^{181}GES loop of the A domain comes above and docks onto the phosphorylation site Asp^{351} by forming an extensive hydrogen-bonding network with the residues of the P domain around Asp^{351}, and thus the T^{181}GES loop sterically blocks the access of the ADP *β*-phosphate to the Asp^{351}-acylphosphate (13). In *E*2PCa$_2$ accumulated in the mutants with the elongated A/M1-linker, the rotation of the A domain and its docking with the P domain for the loss of the ADP-sensitivity must be already achieved as it is ADP-insensitive. Such structural state in *E*2PCa$_2$ was in fact clearly demonstrated by the observation that the tryptic T2 site Arg^{198} on the Val^{200} loop (Asp^{196}-Asp^{203}), another outermost loop of the A domain juxtaposed to the T^{181}GES loop, is completely resistant against tryptic attack as in the *E*2P state without bound Ca^{2+} (Fig. 12).

The elongation of the A/M1-linker markedly accelerated the *E*1PCa$_2$ to *E*2PCa$_2$ isomerization to cause the exclusive accumulation of *E*2PCa$_2$ (Figs. 4 and 5), in contrast, its shortening by a deletion of any single residues blocked this isomerization (23). Therefore, the length of the A/M1-linker needs to be sufficiently long for the *E*1PCa$_2$ to *E*2PCa$_2$ isomerization. The A/M1-linker is probably critical for the positioning of the A domain relative to the P domains, *i.e.* the height from the membrane plane for their docking. Actually in the structural analogs for the ADP-insensitive *E*P (*E*2·MgF_4^{2-} and *E*2·AlF_4^-), the largely rotated A domain is positioned above about half part of the P domain including Asp^{351}, *i.e.* about half of the P domain is located underneath the A domain (Figs. 2 and 13). Hence, the T^{181}GES loop at the lower part of the A domain comes above

Asp^{351} and blocks the access of ADP bound on the N domain to the Asp^{351}-acylphosphate (13).

For realizing the A-P domain association, the P domain also should move significantly from the original position in $E1PCa_2$, *i.e.* incline to the underneath of the A domain. Such motion of the P domain as well as the large rotation of the A domain is probably achieved to produce $E2PCa_2$ at least to some extent to cause their docking and thus the loss of ADP-sensitivity (see footnote 8). (These motions are however still not enough for the subsequent Ca^{2+}-deocclusion/release from $E2PCa_2$ (see next section for the Ca^{2+} release).

As the nature of the wild type, it is known that the *E*P isomerization is a very slow process thus having a kinetic barrier, and this slow process is followed by a very rapid Ca^{2+} release in the scheme in Fig. 1 (actually the isomerization is rate-limiting in the whole Ca^{2+} transport cycle). This means that the isomerization from $E1PCa_2$ to $E2PCa_2$ is accompanied by some structural distortion or strain. Our findings show that such structural restriction for the *E*P isomerization is markedly relieved by the elongation of the A/M1-linker (this study) but markedly enhanced by its shortening (23). The findings further suggest that structural distortion or strain imposed in $E2PCa_2$ upon the *E*P isomerization in the wild type benefits to the work for the subsequent Ca^{2+} release from $E2PCa_2$ (see the next section). This is because virtually no Ca^{2+}-deocclusion/release from $E2PCa_2$ occurred in the mutants with the elongated A/M1-linker. It is tempting to speculate that the largely rotated A domain may be pushed (or even moved) upward upon its positioning above and docking onto the P domain and that such mounting motion could be the structural restriction related to the length of the A/M1-linker.

As a summary of this section, the sufficiently long length of the A/M1-linker is probably critical for the proper motions and positioning of the A and P domains and their docking to produce the $E2PCa_2$ structure in the $E1PCa_2$ to $E2PCa_2$ isomerization. The structural events are markedly accelerated by the elongation of the A/M1-linker, and the structural state of $E2PCa_2$ thus produced with the mutants is very stable, therefore the Ca^{2+}-deocclusion/release from $E2PCa_2$ and the reverse change from $E2PCa_2$ to $E1PCa_2$ are blocked.

Ca^{2+} Release from $E2PCa_2$ after the $E1PCa_2$ to $E2PCa_2$ Isomerization — Our results showed that, after the $E1PCa_2$ to $E2PCa_2$ isomerization, further structural changes should take place with a critical contribution of the A/M1-linker to rearrange the transmembrane helices thereby deocclude Ca^{2+} ions at the transport sites and release into lumen ($E2PCa_2 \rightarrow E2P + 2Ca^{2+}$). Because the elongation of the A/M1-linker blocked the Ca^{2+} deocclusion and release, it is clear that this linker needs to be appropriately short for this event. The structural requirement of the length of the linker is hence in sharp contrast to that for the preceding $E1PCa_2$ to $E2PCa_2$ isomerization, in which the linker needs to be sufficiently long. Our present and previous (23) results clearly showed that 1) the shortening of the A/M1-linker blocks the $E1PCa_2$ to $E2PCa_2$ isomerization, 2) its elongation on the other hand markedly accelerates this isomerization, and 3) its elongation blocks the subsequent Ca^{2+} deocclusion and release from $E2PCa_2$. These results strongly suggest that the A/M1-linker with its native and correct length in the wild type will be strained upon the motion of the A domain and its positioning above half the P domain in the $E1PCa_2$ to $E2PCa_2$ isomerization, and the strain thus imposed in $E2PCa_2$ will be utilized to cause the subsequent structural changes for the Ca^{2+} deocclusion and release, $E2PCa_2 \rightarrow E2P + 2Ca^{2+}$. Then the question is what structural changes are produced by critical contributions of the A/M1-linker with its correct length, *i.e.* its strain, and how the changes are transmitted to the transmembrane region to rearrange the helices to deocclude and release Ca^{2+} by the contribution of the A/M1-linker.

The essential changes of the transmembrane helices for the Ca^{2+} release related with the motions of the cytoplasmic domains are seen in $E1\cdot AlF_x\cdot ADP \rightarrow E2\cdot MgF_4^{2-}$ as the model for the overall

structural change in the *E*P isomerization/Ca^{2+}-release process *E*1PCa_2 → *E*2P + $2Ca^{2+}$. Namely, as described in detail by Toyoshima *et al.* (13, 51), the inclination of the P domain (*i.e.* its moving and tilting to the A domain) causes the sideward shift of the cytoplasmic part of M4 (M4C), downward movement of M4, bending of M5C, and also rotation of M6; these changes would destroy the Ca^{2+}-binding sites. Also critical is the tilting of M2, which forms a V-shaped rigid body structure with M1'/M1 by van der Waals contacts. This rigid body moves (M1' rotates and M2/M1 tilts) as the A domain largely rotates (see Fig. 13 and Figure 4 in Ref. 13). Especially, the top part of M2 at its junction with the A domain largely moves outward, thus M2 largely tilts and pushes against the lumenal half of M4 *via* M1 to open the lumenal gate (13).

Because the A/M1-linker connects directly the A domain with M1'/M1, it would be easy at first glance to assume that this linker functions for transmitting the motion of the A domain directly to the M1'/M1/M2 rigid body to cause its motion, and such linkage would be impaired by the elongation of the A/M1-linker. In more detail in the change *E*1·AlF_x·ADP → *E*2·MgF_4^{2-}, M1' rotates away from its original position as the A domain rotates, the top part of M2 comes to the position where M1' was originally positioned, and the top part of M1 also moves sideward (see Figure 4 in Ref. 13). If the A/M1-linker is elongated, the linker for example can not pull M1'/M1, and the coordination between the motion of the A domain and that of M1'/M1/M2 would be impaired or not enough for the Ca^{2+} deocclusion and release.

Nevertheless, to further clarify the critical structural contributions of the A/M1-linker in the Ca^{2+}-deocclusion/release process, it is necessary to take into account the actual structural difference revealed between *E*2PCa_2 and the Ca^{2+}-released form of *E*2P. Namely, in *E*2PCa_2, the Tyr^{122}-hydrophobic cluster is not properly formed yet as demonstrated by the rapid PrtK-cleavage at Leu^{119} in sharp contrast to its complete resistance with the properly formed cluster in the Ca^{2+}-released form of *E*2P (Fig. 12). Importantly, this cluster is produced by the largely moved three structural elements and their appropriate positioning, *i.e.* by the largely rotated A domain, the largely tilted M2, and the largely inclined P domain (see *E*1·AlF_x·ADP → *E*2·MgF_4^{2-} in Fig. 13). Therefore in the mutants with the elongated A/M1-linker, the motions of these elements are not yet achieved enough to form the cluster and they are not stabilized at the appropriate positions due to the lack of the proper cluster. In this context, it should be noted that our present observations are in accord with the previous mutation studies on this cluster (19, 22) that the formation of this cluster and resulting strong interactions of the three structural elements is critical for the Ca^{2+}-released structure of *E*2P. Actually, in the mutants with the elongated A/M1-linker, the Ca^{2+}-released form of *E*2P or its structural analogs was shown to possess the proper Tyr^{122}-hydrophobic cluster (Fig. 12) and the lumenally opened Ca^{2+}-release pathway (Fig. 10).

All these findings directed us that, for understanding the Ca^{2+}-release process from *E*2PCa_2, it is necessary to further consider and dissect the possible roles of the A/M1-linker in the motions and proper positioning of these three structural elements to form the cluster. This implies even a possible contribution of the A/M1-linker to the motion of the P domain from *E*2PCa_2 to *E*2P. Note that the rearrangements of M4/M5 are essential for the Ca^{2+}-deocclusion/release, and must be linked with the motion of the P domain from the *E*2PCa_2 state because M4/M5 are directly connected with the P domain. As discussed in the above section for the *E*1PCa_2 to *E*2PCa_2 isomerization, in *E*2PCa_2, the half part of the P domain is probably positioned already underneath the A domain and associated with this domain by forming the two interaction networks at the Val^{200} loop and at the T^{181}GES loop. For this A-P domain association in the *E*P isomerization, the P domain may be inclined to some extent (as also described in footnote 8). It is possible that the A/M1-linker with its strain likely functions to cause a further motion of the P domain from

$E2PCa_2$ *via* the associated A domain, thereby accomplishing the rearrangements of M4/M5 required for the Ca^{2+}-deocclusion/release from $E2PCa_2$. It is tempting to speculate that the A domain is pulled by the strain of the A/M1-linker, and pushes down the P domain located underneath the A domain. Thereby the P domain inclines further from the $E2PCa_2$ state, and the residues of this domain (Val^{705}/Val^{726}) come to the position to form the Tyr^{122}-hydrophobic cluster with the A domain (Ile^{179}/Leu^{180}/Ile^{232}) and the top part of M2 (Tyr^{122}/Leu^{119}). Consequently, M4/M5 connected with the P domain will be rearranged to finally destroy the Ca^{2+}-sites and release Ca^{2+}. The formation of the Tyr^{122}-hydrophobic cluster at the bottom part of the A-P domain interface would stabilize this inclined state of the P domain, *i.e.* the Ca^{2+}-released form of $E2P$. The two interaction networks at the upper part of the A-P domain interface (at the Val^{200} loop and at the $T^{181}GES$ loop) may function in $E2PCa_2 \rightarrow E2P + 2Ca^{2+}$ as a base for such final adjustment of the interface of the A and P domains by the contribution of the A/M1-linker.

Regarding the motion of M1'/M1/M2 to achieve the Ca^{2+} release from $E2PCa_2$, the structural state of $E2PCa_2$ accumulated without having the proper Tyr^{122}-hydrophobic cluster is consistent with the view that M2 is not yet tilted enough in $E2PCa_2$ for the Ca^{2+} release and/or that the tilted state (*i.e.* the Ca^{2+}-released state) is not stabilized. Note that Leu^{119} (PrtK-site) and Tyr^{122} on the top part of M2 are involved in formation of this cluster (Fig. 13). As an additional mechanism to accomplish the tilting of M2 for the Ca^{2+} release besides the rotation of the A domain, the inclination of the P domain toward and its colliding with the top part of M2 (thus producing the Tyr^{122}-hydrophobic cluster) might possibly be involved. Namely, such changes would push the top part of M2 outward to cause further its tilting to finally achieve the Ca^{2+} release. As for the critical structural role of the long helix M2, it is important to state that its top part is fixed by the firm interactions with the A and P domain at the Tyr^{122}-hydrophobic cluster and therefore M2 can function for transmitting the motions of the cytoplasmic domains to transmembrane domain by its large tilting, like a lever arm.

In this section, we dissected the possible contributions of the A/M1-linker with its strain to the further motions of the three structural elements from the $E2PCa_2$ state for producing the Ca^{2+}-released structure of $E2P$ with the Tyr^{122}-hydrophobic cluster. *Via* these changes in the cytoplasmic region, the A/M1-linker likely contributes not only to the motions of M1'/M1/M2 but also those of M4/M5 to open the lumenal gate and destroy the Ca^{2+}-sites, hence accomplishing the coordination of these structural events required for the Ca^{2+} deocclusion and release. The elongation of the A/M1-linker probably diminished its strain, and disrupted these structural events and the proper formation of the Tyr^{122}-hydrophobic cluster that stabilizes the Ca^{2+}-released state. $E2PCa_2$ is therefore trapped in the mutants with the elongated linker. As for the two steps mechanism $E1PCa_2 \rightarrow E2PCa_2 \rightarrow E2P + 2Ca^{2+}$, it is of interest to know in future structural studies how far the rearrangements in the cytoplasmic and transmembrane regions actually occur in the first step and further in the second to finally deocclude and release Ca^{2+} from $E2PCa_2$. In the wild type, however, all the structural changes in these processes may be occurring as a series of successive events by the critical contribution of the A/M1-linker, and $E2PCa_2$ may not be trapped as a distinct intermediate.

Possible Role of M1' in Ca^{2+} Release from $E2PCa_2$ — As indicated by the kinetic results, the non-conservative serine substitution of the hydrophobic residues Leu^{49}/Trp^{50}/Leu^{52}/Val^{53}/Ile^{54} on the amphipathic helix M1' (4950525354S) causes the strongly favored $E2PCa_2$ accumulation (Figs. 4 and 5) and blocks the $E2PCa_2$ decay (Figs. 6 and 7). In this regard, the consequence of this mutation is very similar to that of the elongation of the A/M1-linker. M1' is directly connected with the A/M1-linker and lying on the membrane surface, and the hydrophobic residues aligned on M1' probably form interactions with the membrane core thus

anchoring M1' to the membrane (12, 13) (see Fig. 2). Our results therefore suggest that the hydrophobic interactions are important for fixing M1' at the membrane surface and thus for forming a base for the A/M1-linker to restrict its possible dislocation; thereby the strain will be imposed on the linker in $E2PCa_2$ and can be utilized for the Ca^{2+} deocclusion and release from $E2PCa_2$.

E2P Hydrolysis after Ca^{2+} Release — The elongation of the A/M1-linker does not inhibit the rapid hydrolysis of the Ca^{2+}-free form of *E*2P (Fig. 7), in contrast, the shortening of the linker by the deletion of any single residues blocks the hydrolysis as shown previously (23). Therefore, the length of the A/M1-linker needs to be sufficiently long for the Asp^{351}-acylphosphate hydrolysis. The catalytic site for the *E*2P hydrolysis consists of the P and A domains, and the A domain is positioned above about half part of the P domain (see Fig. 13, $E2{\cdot}MgF_4^{2-}$). Hence the T^{181}GES loop of the A domain is situated above Asp^{351} and a water molecule coordinated by Glu^{183} can attack the acylphosphate (13, 14, 52). It is therefore very likely that the A/M1-linker of its sufficiently long length is critical for formation of the correct configuration of the catalytic site from the properly positioned A and P domains, and the shortening of the linker by the deletion of even a single residue disrupted the catalytic site.

Energy Coupling — Regarding the coupling between ATP hydrolysis and Ca^{2+} transport, it is important to note that the Asp^{351}-acylphosphate of the mutants with the elongated A/M1-linker (*i.e.* with the sufficiently long linker) was not hydrolyzed in $E2PCa_2$, by contrast, it was rapidly hydrolyzed in the Ca^{2+}-released form of *E*2P produced from P_i without Ca^{2+} (Figs. 6 and 7). The results indicate that some rearrangement in the A and P domains should take place during the Ca^{2+} release from $E2PCa_2$ to produce the catalytic site with the hydrolytic function. As described above, the structural difference between these two states is that the Tyr^{122}-hydrophobic cluster is not formed properly yet in $E2PCa_2$ but present in the Ca^{2+}-released *E*2P state. These observations are actually in complete agreement with the previous finding by the mutation studies (19, 22) that the formation of the Tyr^{122}-hydrophobic cluster is critical for formation of the catalytic site for the acylphosphate hydrolysis in *E*2P. In fact, the T^{181}GES loop in the catalytic site is at the immediate C-terminus of Ile^{179}/Leu^{180} of the Tyr^{122}-hydrophobic cluster, and the DGV^{705}ND loop that coordinates catalytic Mg^{2+} has Val^{705} of the cluster (for details of the structure, see Supplemental Figure II in Ref. 19). As described above, the formation of this cluster is most probably critical also for the Ca^{2+}-deocclusion/release from $E2PCa_2$. In fact, the Ca^{2+}-released form of *E*2P produced from P_i in the mutants was shown to possess the lumenally opened Ca^{2+}-release pathway (Fig. 10) as well as the catalytic site with the normal hydrolytic activity (Fig. 7). Thus, the Tyr^{122}-hydrophobic cluster formed with the critical contribution of the A/M1-linker functions both for the Ca^{2+}-deocclusion/release at the transport sites and for the formation of the catalytic site with the hydrolytic activity. Importantly, as a consequence of this structural mechanism, a possible acylphosphate hydrolysis in $E2PCa_2$ without releasing Ca^{2+} will be avoided, and hence the reaction sequence for the Ca^{2+} release and subsequent acylphosphate hydrolysis will be ensured and thus accomplishing the energy coupling in the Ca^{2+} transport.

During the *E*2P hydrolysis to *E*2, the lumenal Ca^{2+} gate should be closed and the ATPase prevents possible Ca^{2+} leakage from lumen. On the basis of the structural change $E2{\cdot}MgF_4^{2-} \rightarrow E2(TG)$, it was predicted (13) that the lumenal gate-closure involves the release of the A domain from the P domain (the loss of the interactions at the T^{181}GES loop and Val^{200} loop regions) and a tilting of the A domain upon the dephosphorylation (see Figure 6 in Ref. 13). An interesting and specific question for us here was whether the strain of the A/M1-linker possibly contributes to the tilting of the A domain during the *E*2P hydrolysis and thus to the closure of the lumenal gate. But this seems unlikely. This is because the rate in the *E*2P hydrolysis and

the Ca^{2+} affinity and rate in the *E*2 to *E*1Ca_2 transition in the mutants with the elongated A/M1-linker are normal (Fig. 7 and Table I) and therefore the normal structural changes probably take place during the *E*2P hydrolysis to *E*2 in the mutants as in the wild type.

Finally, it is worth noting that the strain of the A/M3-linker has been predicted to be important for the large rotation of the A domain in the *E*P isomerization (13, 53). The A/M1-linker, the A/M2-linker (top part of M2) including Tyr^{122}/Leu^{119}, and the A/M3-linker therefore play distinct structural roles for the successive structural events in the *E*1PCa_2 to *E*2PCa_2 isomerization, the Ca^{2+}-deocclusion/release, and the *E*2P hydrolysis. In the transport cycle, the energy gained by the Ca^{2+}- and ATP-bindings will be transformed into the structural states of the phosphorylated intermediates producing the strain of the linkers and the motions and strong interactions of the A and P domains, and the conformational energy thus produced is utilized for the structural changes to deocclude and release Ca^{2+} into lumen. The usefulness for the Ca^{2+}-ATPase having flexible links between cytoplasmic domains and the transmembrane domain are also discussed extensively in the very recent paper by Toyoshima *et al.* (51).

In summary, our studies revealed the structural requirements of the length of the A/M1-linker. The linker needs to be 1) sufficiently long for the *E*1PCa_2 to *E*2PCa_2 isomerization, 2) appropriately short for the subsequent Ca^{2+} deocclusion and release, *E*2PCa_2 → *E*2P + $2Ca^{2+}$, and 3) then again sufficiently long for the *E*2P hydrolysis, *E*2P + H_2O → *E*2 + P_i. The native length of the A/M1-linker in the wild type is therefore precisely designed for inducing and coordinating the successive structural events in these steps and for the energy coupling. On the basis of the results and structures, we dissected the structural events for these processes and the functions of the structural elements involved in the processes.

Acknowledgments — We would like to thank Dr. David H. MacLennan, University of Toronto, for his generous gift of SERCA1a cDNA and Dr. Randal J. Kaufman, Genetics Institute, Cambridge, MA, for his generous gift of the expression vector pMT2. We are also grateful to Dr. Chikashi Toyoshima, University of Tokyo, for helpful discussions.

REFERENCES

1. Hasselbach, W., and Makinose, M. (1961) *Biochem. Z.* **333,** 518–528
2. Ebashi, S., and Lipmann, F. (1962) *J. Cell Biol.* **14,** 389–400
3. Inesi, G., Sumbilla, C., and Kirtley, M. E. (1990) *Physiol. Rev.* **70,** 749–776
4. Møller, J. V., Juul, B., and le Maire, M. (1996) *Biochim. Biophys. Acta* **1286,** 1–51
5. MacLennan, D. H., Rice, W. J., and Green, N. M. (1997) *J. Biol. Chem.* **272,** 28815–28818
6. McIntosh, D. B. (1998) *Adv. Mol. Cell. Biol.* **23A,** 33–99
7. Toyoshima, C., and Inesi, G. (2004) *Annu. Rev. Biochem.* **73,** 268–292
8. Inao, S., and Kanazawa, T. (1986) *Biochim. Biophys. Acta* **857,** 28-37
9. Toyoshima, C., Nakasako, M., Nomura, H., and Ogawa, H. (2000) *Nature* **405,** 647–655
10. Toyoshima, C., and Nomura, H. (2002) *Nature* **418,** 605–611
11. Sørensen, T. L-M., Møller, J. V., and Nissen, P. (2004) *Science* **304,** 1672–1675
12. Toyoshima, C., and Mizutani, T. (2004) *Nature* **430,** 529–535
13. Toyoshima, C., Nomura, H., and Tsuda, T. (2004) *Nature* **432,** 361–368
14. Olesen, C., Sørensen, T. L.-M., Nielsen, R. C., Møller, J. V., and Nissen, P. (2004) *Science* **306,** 2251–2255
15. Danko, S., Daiho, T., Yamasaki, K., Kamidochi, M., Suzuki, H., and Toyoshima, C. (2001) *FEBS Lett.* **489,** 277–282
16. Danko, S., Yamasaki, K., Daiho, T., Suzuki, H., and Toyoshima, C. (2001) *FEBS Lett.* **505,**

129–135
17. Danko, S., Yamasaki, K., Daiho, T., and Suzuki, H. (2004) *J. Biol. Chem.* **279,** 14991–14998
18. Clarke, D. M., Loo, T. W., and MacLennan, D. H. (1990) *J. Biol. Chem.* **265,** 14088–14092
19. Wang, G., Yamasaki, K., Daiho, T., and Suzuki, H. (2005) *J. Biol. Chem.* **280,** 26508–26516
20. Anthonisen, N., Clausen, J. D., and Andersen, J. P. (2006) *J. Biol. Chem*. **281**, 31572–31582
21. Kato, S., Kamidochi, M., Daiho, T., Yamasaki, K., Wang, G., and Suzuki, H. (2003) *J. Biol. Chem.* **278,** 9624–9629
22. Yamasaki, K., Daiho, T., Danko, S., and Suzuki, H. (2004) *J. Biol. Chem.* **279,** 2202–2210
23. Daiho, T., Yamasaki, K., Wang, G., Danko, S., Iizuka, H., and Suzuki, H. (2003) *J. Biol. Chem.* **278,** 39197–39204
24. Kaufman, R. J., Davies, M. V., Pathak, V. K., and Hershey, J. W. B. (1989) *Mol. Cell. Biol.* **9,** 946–958
25. Maruyama, K., and MacLennan, D. H. (1988) *Proc. Natl. Acad. Sci. U. S. A.* **85,** 3314–3318
26. Daiho, T., Yamasaki, K., Suzuki, H., Saino, T., and Kanazawa, T. (1999) *J. Biol. Chem.* **274,** 23910–23915
27. Kanazawa, T., Saito, M., and Tonomura, Y. (1970) *J. Biochem.* (*Tokyo*) **67,** 693–711
28. Weber, K., and Osborn, M. (1969) *J. Biol. Chem.* **244,** 4406–4412
29. Daiho, T., Suzuki, H., Yamasaki, K., Saino, T., and Kanazawa, T. (1999) *FEBS Lett.* **444,** 54–58
30. Sagara, Y., Wade, J. B., and Inesi, G. (1992) *J. Biol. Chem.* **267,** 1286–1292
31. Laemmli, U. K. (1970) *Nature* **277,** 680–685
32. Lowry, O. H., Rosebrough, N. J., Farr, A. L., and Randall, R. J. (1951) *J. Biol. Chem.* **193,** 265–275
33. Humphrey, W., Dalke, A., and Schulten, K. (1996) *J. Mol. Graphics* **14,** 33–38
34. Einholm, A. P., Vilsen, B., and Andersen, J. P. (2004) *J. Biol. Chem.* **279,** 15888–15896
35. Pick, U., and Karlish, S. J. D. (1982) *J. Biol. Chem.* **257,** 6120–6126
36. Shigekawa, M., and Dougherty, J. P. (1978) *J. Biol. Chem.* **253,** 1451–1457
37. Inesi, G., Kurzmack, M., and Lewis, D. (1988) *Methods Enzymol.* **157,** 154–190
38. de Meis, L., Martins, O. B., and Alves, E. W. (1980) *Biochemistry* **19,** 4252–4261
39. de Meis, L., and Inesi, G. (1982) *J. Biol. Chem.* **257,** 1289–1294
40. Sato, K., Yamasaki, K., Daiho, T., Miyauchi, Y., Takahashi, H., Ishida-Yamamoto, A., Nakamura, S., Iizuka, H., and Suzuki, H. (2004) *J. Biol. Chem.* **279,** 35595–35603
41. Nakamura, Y. (1984) *J. Biol. Chem.* **259,** 8183–8189
42. Nakamura, Y., Kurzmack, M., and Inesi, G. (1986) *J. Biol. Chem.* **261,** 3090–3097
43. Prager, R., Punzengruber, C., Kolassa, N., Winkler, F., and Suko, J. (1979) *Eur. J. Biochem.* **97,** 239–250
44. Hanel, A. M., and Jencks, W. P. (1991) *Biochemistry* **30,** 11320–11330
45. Sagara, Y., Fernandez-Belda, F., de Meis, L., and Inesi, G. (1992) *J. Biol. Chem.* **267,** 12606–12613
46. Xu, C., Ma, H., Inesi, G., Al-Shawi, M. K., and Toyoshima, C. (2004) *J. Biol. Chem.* **279,** 17973–17979
47. Seekoe, T., Peall, S., and McIntosh, D. B. (2001) *J. Biol. Chem.* **276,** 46737–46744
48. Juul, B., Turc, H., Durand, M.L., Gomez de Gracia, A., Denoroy, L., Møller, J. V., Champeil, P. and le Maire, M. (1995) *J. Biol. Chem.* **270,** 20123–20134
49. Lenoir, G., Picard, M., Gauron, C., Montigny, C., Le Maréchal, P., Falson, P., le Maire, M., Møller, J. V., and Champeil, P. (2004) *J. Biol. Chem.* **279,** 9156–9166
50. Myung, J., and Jencks, W. P. (1995) *Biochemistry* **34,** 3077–3083
51. Takahashi, M., Kondou, Y., and Toyoshima, C. (2007) *Proc. Natl. Acad. Sci. U. S. A.* **104,** 5800–5805
52. Clausen, J. D., Vilsen, B., McIntosh, D. B., Einholm, A. P., and Andersen, J. P. (2004) *Proc. Natl. Acad. Sci. U. S. A.* **101,** 2776–2781

53. Møller, J. V., Lenoir, G., Marchand, C., Montigny, C., le Maire, M., Toyoshima, C., Juul, B. S., and Champeil, P. (2002) *J. Biol. Chem.* **277,** 38647–38659
54. Shigekawa, M., Wakabayashi, S., and Nakamura, H. (1983) *J. Biol. Chem.* **258,** 8698–8707
55. Wakabayashi, S., and Shigekawa, M. (1987) *J. Biol. Chem.* **262,** 11524–11531
56. Picard, M., Toyoshima, C., and Champeil, P. (2005) *J. Biol. Chem.* **280,** 18745–18754
57. Picard, M., Jensen, A.-M. L., Sørensen, T. L.-M., Champeil, P., Møller, J. V., and Nissen, P. (2007) *J. Mol. Chem.* **368,** 1–7
58. Froehlich, J. P., and Heller, P. F. (1985) *Biochemistry* **24,** 126–136
59. Mahaney, J. E., Thomas, D. D., and Froehlich, J. P. (2004) *Biochemistry* **43,** 4400–4416

FOOTNOTES

*This work was supported by Grant-in-Aid for Scientific Research (C) (to T.D.) and (B) (to H.S.) from the Ministry of Education, Culture, Sports, Science and Technology of Japan, and in part by a Creative Science Project Grant (to H.S. and Dr. Chikashi Toyoshima (Head Investigator of the Grant), University of Tokyo) from the Ministry of Education, Culture, Sports, Science and Technology of Japan.

[1]To whom correspondence should be addressed: Dept. of Biochemistry, Asahikawa Medical College, Midorigaoka-higashi, Asahikawa, 078-8510, Japan. Tel.: 81-166-68-2350; Fax: 81-166-68-2359; E-mail: daiho@asahikawa-med.ac.jp.

[2]The abbreviations used are: SERCA1a, adult fast-twitch skeletal muscle sarcoplasmic reticulum Ca^{2+}-ATPase; SR, sarcoplasmic reticulum; *E*P, phosphoenzyme; *E*1P, ADP-sensitive phosphoenzyme; *E*2P, ADP-insensitive phosphoenzyme; TG, thapsigargin; MOPS, 3-(*N*-morpholino)propanesulfonic acid; MES, 2-(*N*-morpholino)ethanesulfonic acid; V_i, orthovanadate; PrtK, proteinase K.

[3]In this regard, we should describe the reasons why we chose the positions 42/43 and 46/47 for the insertions. First of all, to explore the importance of the length of the linker and to assign the effects of the insertions straightforwardly as those of the elongation of the linker, it is necessary or better to have insertions (at least) at two different positions. Then for the choice of the two, the positions approximately at one third and at two thirds of the length of the linker would be reasonable because the A/M1-linker, Glu^{40}-Ser^{48} loop, is an extended loop without helical structure (see Fig. 2) and has no extensive interactions with other parts of the ATPase molecule (actually the substitutions of any single residues in this loop did not impair the function (23)). Also, the two positions should be not too close to the junctions of the A/M1-linker with the A domain and with M1' (and to the membrane lipids). This is to avoid possible disruption of the structures at the junctions. With these reasons, we chose the two insertion-positions at 42/43 and 46/47, and thereby distributed the two on the linker but not concentrate them very close to each other at the middle part or at either side of the linker. As a reason for the choice of glycine(s) as the amino acid for the insertions, we intended to minimize possible disruption of the extended loop-structure of the linker and to avoid possible formation of side-chain interactions. The results in Fig. 3 of the mutants with the insertions at the two different positions therefore agree with the view that the observed effects are due to the elongation of the A/M1-linker. The kinetic analysis shown in the following figures further revealed that the properties of the mutants with the insertions at the two different positions are essentially the same.

[4]The details of the experimental conditions are as follows: *E*2P was first formed from non-radioactive P_i in 35% (v/v) Me_2SO in the absence and presence of 1 μM thapsigargin (TG), otherwise as in Fig. 9. Subsequently, the mixture was diluted 10-fold at 0 °C with a solution containing 3 mM $^{45}CaCl_2$, 1 μM A23187, 0.1 M KCl, 7 mM $MgCl_2$, and 50 mM MOPS/Tris (pH 7.0), and incubated for 1 min. This mixture was further diluted 10-fold with a "washing solution" containing 20 mM EGTA, 1 μM A23187, 0.1 M KCl, 7 mM $MgCl_2$, and 50 mM MOPS/Tris (pH 7.0),

and incubated for 3 min for hydrolyzing the Ca^{2+}-unbound fraction of *E*2P (see Figs. 7 and 10) and for reducing non-specifically bound Ca^{2+}. The mixture was then subjected to the membrane filtration with the extensive washing by the above EGTA-containing washing solution, otherwise as described in Fig. 8.

[5]Regarding the wild type, the observed biphasic behavior in the *E*P decay after the addition of the high concentrations of Ca^{2+} in Fig. 10*A* may not be accounted for if we assume a rapid equilibrium in the reaction $E1PCa_2 \leftrightarrow E2PCa_2 \leftrightarrow E2P + 2Ca^{2+}$ under these conditions, *i.e.* in the presence of high Ca^{2+} concentrations (because if in the rapid equilibrium, a slowed (but still) single exponential decay after the addition of Ca^{2+} may be expected). In this regard, it may be of interest to note that, in the previous analysis with SR Ca^{2+}-ATPase by Nakamura and Inesi *et al.* (41, 42) for the decay of $E1PCa_2$ formed from ATP, a biphasic $E1PCa_2$ decay with a markedly slowed decay in second phase at the high lumenal Ca^{2+} concentrations was well documented, and actually the $E1PCa_2$ fraction in the second phase was increased with the increase in the Ca^{2+} concentrations at sub-mM to ~mM. To account for the biphasic decay, Inesi *et al.* proposed the branched reaction mechanism from $E1PCa_2$ to $E2PCa_2$ (42), in which $E1PCa_2$ rapidly decays in the presence of bound ADP, but very slowly in its absence and in the presence of the high concentrations of Ca^{2+}. As a reason for the retardation of the $E1PCa_2$ decay at the high Ca^{2+} concentrations in Fig. 10*A*, it is also possible that Mg^{2+} bound at the catalytic metal site in $E1PCa_2$ was substituted by Ca^{2+}, and hence the *E*P isomerization (thus the $E1PCa_2$ decay) was markedly slowed due to this bound Ca^{2+}, as demonstrated previously by using the substrate CaATP with SR Ca^{2+}-ATPase (54, 55). The marked stabilization of the structure of the $E1PCa_2$ state by Ca^{2+} bound at the catalytic site was actually demonstrated by the recent structural studies on its analogs with SR Ca^{2+}-ATPase (56, 57).

[6]In this regard, we would like to make the following two additional discussions in relation to previously proposed mechanisms: Firstly, the standard view on the reaction mechanism with the sequential occurrence of *E*1P and *E*2P in the linear kinetic model (see Fig. 1) has been challenged, and instead an "out-of-phase coupling of the catalytic reactions" in the interacting ATPase molecules in their dimer was postulated (58, 59). In this model, one ATPase molecule in the dimer proceeds the catalytic steps one step ahead of the other, and therefore the presence of equimolar steady-state concentrations of $E1PCa_2$ and $E2PCa_2$ are expected to be observed. On the other hand, in the present study with the mutants with the elongated A/M1-linker, we observed clearly the exclusive accumulation of $E2PCa_2$ (*E*2P possessing the stoichiometric amount of occluded Ca^{2+}) among all the *E*P present at the steady state with no $E1PCa_2$. Actually, in more detail in Figs. 4-6 and 8, almost all of *E*P accumulated at steady state with the wild type was $E1PCa_2$, and the accumulation of the stable $E2PCa_2$ increased with the increase in the number of the inserted glycines in the A/M1-linker (*i.e.* 50% $E2PCa_2$ with 50% $E1PCa_2$ in 2Gi-46/47, and nearly 100% $E2PCa_2$ in the mutants with 3 or more glycines-insertion). Thus, at least in our system in the present study, the postulated out-of-phase coupling of the catalytic reactions is unlikely, or it might be possible that the postulated interactions between the ATPase molecules are disrupted in the mutants. As the second point of the additional discussions, the presence of a slow step in the reverse transition *E*2P to $E1PCa_2$ upon the lumenal Ca^{2+} binding to *E*2P has also been a subject of controversy, and the mere presence of $E2PCa_2$ has been questioned (50). Jencks *et al.* concluded on the basis of the observed very rapid reverse transition (50) that there is no kinetic barrier in this reversal $E2P + 2Ca^{2+} \rightarrow E1PCa_2$, and that there is only one phosphorylated intermediate with bound Ca^{2+} in the transport cycle (*i.e.* $E1PCa_2$). This reversal in the wild type upon the lumenal Ca^{2+} binding to *E*2P is certainly very rapid (as the kinetic results in Fig. 10*A* with the wild type indicated). On the other hand, in the present study with the mutants with the elongated A/M1-linker, we also found the exclusive accumulation of $E2PCa_2$ in the reverse reaction from *E*2P and Ca^{2+} as well as in the forward reaction with ATP and Ca^{2+}. Thus for the first time, we were able to trap the intermediate state $E2PCa_2$ by introducing the mutations, and thereby we identified the structural element that is critical for the Ca^{2+} release from $E2PCa_2$ and for the rapid reverse transition from $E2PCa_2$ to $E1PCa_2$. It should be noted, however, that in the wild type all the

structural changes in these processes may be occurring as successive events, therefore, the intermediate state $E2PCa_2$ may not be trapped or detected as a stable one.

[7]The shortening of the A/M1-linker by the deletion of single residues (Ref. 23) and its elongation by the one to four glycines-insertions (this study) did not cause serious consequences on the $E2$ to $E1Ca_2$ transition and the $E1PCa_2$ formation from $E1Ca_2$ and ATP, therefore on the structural changes in these steps.

[8]It is important to note that, in all the crystal structures $E1Ca_2$, $E1{\cdot}AlF_x{\cdot}ADP$, $E2{\cdot}AlF_4^-$, $E2{\cdot}MgF_4^{2-}$, and $E2$(TG), Arg^{334}/Arg^{324} at the bottom part of the P domain forms an ionic and hydrogen-bonding interaction network with the top part of M2 (the A/M2-linker region) where the several polar and negatively charged residues are aligned ($Glu^{123}/Glu^{121}/Glu^{117}/Asn^{114}/Glu^{113}/Asn^{111}/Glu^{109}/Gln^{108}$). In the change $E1{\cdot}AlF_x{\cdot}ADP \rightarrow E2{\cdot}MgF_4^{2-}$ or $E2{\cdot}AlF_4^-$, Arg^{334} moves downward from the Glu^{123}/Glu^{121}-region to Asn^{114}/Asn^{111} in the interaction network (see Figure 8 in Ref. 22). The structures therefore suggest that the interactions in the network may function as to guide and pull the P domain to cause its inclination toward the underneath of the A domain when the A domain largely rotates and M2 tilts away. Importantly, the mutations in this interaction network involving Arg^{324}/Arg^{334} were previously found to block the loss of the ADP-sensitivity, *i.e.* the $E1PCa_2$ to $E2PCa_2$ isomerization (22). Therefore, the inclination of the P domain occurs to some extent during the $E1PCa_2$ to $E2PCa_2$ isomerization. The strain of the A/M1-linker imposed in $E2PCa_2$ likely causes further inclination of the P domain in $E2PCa_2 \rightarrow E2P + 2Ca^{2+}$ as the final process. Thereby the A-P domain interface is further adjusted to achieve the Ca^{2+}-deocclusion/release, and Val^{705}/Val^{726} of the P domain reaches $Ile^{179}/Leu^{180}/Ile^{232}$ of the A domain and Tyr^{122}/Leu^{119} on the top part of M2 producing the Tyr^{122}-hydrophobic cluster, which is critical for stabilizing the Ca^{2+}-released structure of $E2P$.

FIGURE LEGENDS

FIGURE 1. **Ca^{2+} transport cycle of SERCA.**

FIGURE 2. **Structure of SERCA1a.** (*a*) the structural model for the change $E1PCa_2 \rightarrow E2P + 2Ca^{2+}$ was depicted with $E1{\cdot}AlF_x{\cdot}ADP$ ($E1PCa_2{\cdot}ADP$ analog) and $E2{\cdot}MgF_4^{2-}$ ($E2{\cdot}P_i$ analog) (13, 17, PDB accession code 1WPE and 1WPG, respectively). The cytoplasmic three domains N, P, and A are *green*, *pink*, and *yellow*. The transmembrane helices (M1~M10) are numbered, and some are colored. The two structures were manually fitted with M8-M10, which do not move virtually in the two structures. In $E1{\cdot}AlF_x{\cdot}ADP$, the two Ca^{2+} ions bound at their binding (transport) sites are depicted (*red spheres*); the sites consist of the residues on M4, M5, M6, and M8. The linkers connecting the A domain with M1 (*A/M1-linker* with *red*), with M2 (*A/M2-linker* with *green*), and with M3 (*A/M3-linker* with *gray*) are indicated. The *arrows* on $E1{\cdot}AlF_x{\cdot}ADP$ with *yellow*, *pink*, and *blue* show the movements of the A domain, the P domain, and M1', respectively, in the change $E1{\cdot}AlF_x{\cdot}ADP \rightarrow E2{\cdot}MgF_4^{2-}$. The phosphorylation site Asp^{351}, AlF_x, and MgF_4^{2-} are shown, but ADP was not depicted for simplicity. The specific cleavage sites for trypsin (*T2*, Arg^{198} on the Val^{200} loop (Asp^{196}-Asp^{203}); *T1*, Arg^{505}) and proteinase K (*PrtK*, Leu^{119}) are indicated on $E1{\cdot}AlF_x{\cdot}ADP$. The *semitransparent spheres* on $E2{\cdot}MgF_4^{2-}$ with *purple*, *blue*, and *orange* indicate the three contact regions between the A and P domains, *i.e.* at the T^{181}GES loop (*purple loop* with *TGES*) with the residues around Asp^{351}, at the Val^{200} loop including Arg^{198} (*dark blue loop*) with the polar residues of the P domain ($Arg^{678}/Glu^{680}/Arg^{656}/Asp^{660}$), and at Tyr^{122}/Leu^{119}. Tyr^{122} and Leu^{119} on the top part of M2 (A/M2-linker region) form the interaction network "Tyr^{122}-hydrophobic cluster" with $Ile^{179/}Leu^{180}/Ile^{232}$ of the A domain and Val^{705}/Val^{726} of the P domain (see Fig. 13). Details of the other two interaction regions are also not depicted for simplicity (see Supplemental Figures II and III in Ref. 19 for the details). (*b*) in $E2{\cdot}MgF_4^{2-}$, the regions at the A/M1-linker (Glu^{40}-Ser^{48}, *red*), M1' (Leu^{49}-Asp^{59}, *blue*), M1 (*blue*), and the N-terminal neighbor of the A/M1-linker (*yellow*) are depicted. The sites for the insertion-mutations made in this study are at Gly^{46}/Lys^{47} (between Gly^{46} and Lys^{47})

and Pro^{42}/Ala^{43} on the A/M1-linker and at Thr^{22}/Gly^{23} (as indicated with the α-carbons in *pink spheres*), and at Val^{53}/Ile^{54} on M1'.

FIGURE 3. **Ca^{2+}-ATPase activities of expressed SERCA1a.** The Ca^{2+}-ATPase activity of expressed SERCA1a was determined as described under "Experimental Procedures." The activities are represented as percentage of that of the wild type (1.2 ± 0.1 μmol/min/mg of SERCA1a protein (n = 6)). The values presented are the mean ± S.D. (n = 3-4). 1Gi-46/47~6Gi-46/47 represent the mutants with one to six glycine(s)-insertion between Gly^{46} and Lys^{47}. Likewise, 1Gi-42/43 and 4Gi-42/43 are for the mutants with one and four glycine(s)-insertion between Pro^{42} and Ala^{43}, respectively; 4Ai-22/23 and 4Ai-53/54 are for the mutants with four alanines-insertion between Thr^{22} and Gly^{23} and between Val^{53} and Ile^{54}, respectively. In the mutant 4950525354S, Leu^{49}/Trp^{50}/Leu^{52}/Val^{53}/Ile^{54} on M1' are all substituted by serine. In the mutant 5155565859A, Glu^{51}/Glu^{55}/Gln^{56}/Glu^{58}/Asp^{59} on M1' are all substituted by alanine.

FIGURE 4. **Total amount of *E*P formed from ATP at steady state and the amount of ADP-insensitive *E*P.** Microsomes expressing the wild-type or mutant SERCA1a were phosphorylated with [γ-^{32}P]ATP at 0 °C for 1 min in 50 μl of a mixture containing 1 μg of microsomal protein, 10 μM [γ-^{32}P]ATP, 1 μM A23187, 0.1 M KCl, 7 mM $MgCl_2$, 0.55 mM $CaCl_2$, 0.5 mM EGTA, and 50 mM MOPS/Tris (pH 7.0). The total amount of *E*P formed (*open bars*) was determined by the acid-quenching as described under "Experimental Procedures." For determination of ADP-insensitive *E*P (*closed bars*), an equal volume of a mixture (50 μl) containing 4 mM ADP, 1 μM A23187, 0.1 M KCl, 7 mM $MgCl_2$, 10 mM EGTA, and 50 mM MOPS/Tris (pH 7.0) was added to the above phosphorylation mixture, and the reaction was quenched at 1 s after the ADP addition. ADP-sensitive *E*P (*E*1P) disappeared entirely within 1 s after the ADP addition.

FIGURE 5. **Time course of accumulation of ADP-insensitive *E*P.** Microsomes expressing the wild-type or mutant SERCA1a were phosphorylated with [γ-^{32}P]ATP at 0 °C for various periods as indicated on the abscissa in 50 μl of a mixture containing 1 μg of microsomal protein, 10 μM [γ-^{32}P]ATP, 1 μM A23187, 7 mM $MgCl_2$, 0.55 mM $CaCl_2$, 0.5 mM EGTA, and 50 mM MOPS/Tris (pH 7.0) in the presence of 0.1 M LiCl without added KCl (*A*, *B*) or 0.1 M KCl without LiCl (*C*, *D*). The reaction was quenched by acid and the total amount of *E*P (*A*, *C*) was determined. For determination of ADP-insensitive *E*P (*B*, *D*), an equal volume (50 μl) of a mixture containing 4 mM ADP, 1 μM A23187, 7 mM $MgCl_2$, 10 mM EGTA, 50 mM MOPS/Tris (pH 7.0), and 0.1 M LiCl without KCl (*B*) or 0.1 M KCl without LiCl (*D*) was added to the above phosphorylation mixture at the indicated time. At 1 s after the ADP addition, the reaction was quenched by acid. *Solid lines* show the least squares fit to a single exponential, and the apparent rates to reach the steady-state level are given in Table I. The maximum values of the total amount of *E*P obtained at infinite time in the fitting are normalized to 100% (*A*, *C*) and the amounts of the ADP-insensitive *E*P are shown as percentages of the maximum value of the total amount of *E*P (*B*, *D*).

FIGURE 6. **Decay of *E*P formed from ATP and the fraction of the ADP-insensitive *E*P during the decay.** Microsomes expressing the wild-type or mutant SERCA1a were phosphorylated at 0°C for 1 min in 50 μl of a mixture containing 1 μg of microsomal protein, 10 μM [γ-^{32}P]ATP, 1 μM A23187, 0.1 M KCl, 7 mM $MgCl_2$, 0.55 mM $CaCl_2$, 0.5 mM EGTA, and 50 mM MOPS/Tris (pH 7.0). Phosphorylation was terminated by addition of an equal volume (50 μl) of a buffer containing 10 mM EGTA, 0.1 M KCl, 7 mM $MgCl_2$, and 50 mM MOPS/Tris (pH 7.0) at 0°C. The total amount of *E*P remaining after the EGTA addition was determined by the acid-quenching at the indicated time (*A*). The total amounts of *E*P obtained at zero time (*i.e.* immediately before the EGTA addition) are normalized to 100%. *Solid lines* show the least squares fit to a single exponential, and the decay rates thus obtained are given in Table I. For determination of ADP-insensitive *E*P (*B*), an equal

volume (100 μl) of a mixture containing 4 mM ADP, 1 μM A23187, 0.1 M KCl, 7 mM $MgCl_2$, 10 mM EGTA, and 50 mM MOPS/Tris (pH 7.0) was added to the above EGTA-added phosphorylation mixture at the indicated time. At 1 s after the ADP addition, the reaction was quenched by acid. The amount of the ADP-insensitive *E*P at each of the indicated time thus determined is shown as percentage of the total amount of *E*P determined at zero time.

FIGURE 7. **Hydrolysis of *E*2P formed from P_i without Ca^{2+}.** Microsomes expressing the wild-type or mutant SERCA1a were phosphorylated with $^{32}P_i$ at 25 °C for 10 min in 5 μl of a mixture containing 1 μg of microsomal protein, 0.1 mM $^{32}P_i$, 1 μM A23187, 1 mM EGTA, 10 mM $MgCl_2$, 50 mM MOPS/Tris (pH 7.0), and 35% (v/v) Me_2SO. The mixture was then cooled and diluted at 0 ºC by addition of 95 μl of a mixture containing 2.1 mM non-radioactive P_i, 105 mM KCl, 1 mM EGTA, 10 mM $MgCl_2$, and 50 mM MOPS/Tris (pH 7.0). At different times after the dilution, the *E*2P hydrolysis was quenched by acid. The amounts of *E*2P formed with $^{32}P_i$ at zero time are normalized to 100%. *Solid lines* show the least squares fit to a single exponential, and the rates thus obtained are given in Table I.

FIGURE 8. **Occlusion of Ca^{2+} in *E*P formed from ATP and Ca^{2+}.** (*A*) Microsomes expressing the mutant 4Gi-46/47 were phosphorylated for 10 s with ATP and $^{45}Ca^{2+}$ at 25 °C in 50 μl of a mixture containing 2 μg of microsomal protein, 1 μM ATP, 10 μM $^{45}CaCl_2$, 0.1 M KCl, 7 mM $MgCl_2$, and 30 mM MOPS/Tris (pH 7.0) in the presence (▲) or absence (Δ) of 1 μM A23187. Then a small volume of EGTA was added to give 2 mM to terminate the phosphorylation. At the indicated time after this EGTA addition, the mixture was diluted at 25 °C by 2 ml of a washing solution containing 5 μM A23187, 0.1 M KCl, 7 mM $MgCl_2$, 2 mM EGTA, and 50 mM MOPS/Tris (pH 7.0), and immediately filtered through a 0.45-μm nitrocellulose membrane filter. The samples on the filter were rapidly washed 4 times by 2 ml of the above washing solution at 25 °C. The amount of $^{45}Ca^{2+}$ specifically bound to the expressed SERCA1a, *i.e.* the occluded Ca^{2+} in SERCA1a, was determined after this extensive washing by subtracting the amount of nonspecific Ca^{2+}-binding, which was determined by including 1 μM thapsigargin (TG) in the above phosphorylation mixture, otherwise as described under "Experimental Procedures." The values are shown as "nmol per mg of SERCA1a applied on the filter" (Δ, ▲). By using [γ-^{32}P]ATP and non-radioactive $CaCl_2$, the total amount of *E*P present in the above EGTA-added phosphorylation mixture was determined at the indicated time by acid-quenching (*open* and *closed diamonds*). *E*P present was found to be exclusively the ADP-insensitive one (*E*2P) as also demonstrated with this mutant in Figs. 4-6. The amounts of *E*P were also determined without the acid-quenching but with the membrane filtration method as the above determination of the occluded $^{45}Ca^{2+}$. The amounts of *E*P thus determined by the two methods actually agreed well with each other, and therefore the acid-quenching method was employed throughout the experiments in (*A*) and (*B*) for convenience. (*B*) Microsomes expressing the mutant 2Gi-46/47 were phosphorylated with ATP and $^{45}Ca^{2+}$ in the presence of 1 μM A23187 at 10 °C otherwise as described in (*A*). The phosphorylation was terminated by the EGTA addition as in (*A*), and at the indicated time after this EGTA addition, the mixture was diluted at 10 °C by 2 ml of a washing solution containing 1 μM A23187, 0.1 M KCl, 7 mM $MgCl_2$, 2 mM EGTA, and 50 mM MOPS/Tris (pH 7.0) in the presence (●) or absence (○) of 2 mM ADP. The sample was immediately filtered through the membrane filter, washed 4 times by 2 ml of the washing solution with (●) and without (○) ADP at 10 °C, and the amount of bound $^{45}Ca^{2+}$ was determined. By using [γ-^{32}P]ATP and non-radioactive $CaCl_2$, the total amount of *E*P (□) and the amount of ADP-insensitive *E*P (■) present in the above EGTA-added phosphorylation mixture were determined at the indicated time. (*C*) The stoichiometry of Ca^{2+} occluded in *E*P was calculated at each time points in the *E*P decay in *A* and *B*. The mutants 4Gi-46/47 and 2Gi-46/47, and the conditions employed are indicated with different symbols in the figure.

FIGURE 9. **Formation of stable *E*2P in the reverse reaction by addition of high concentration of Ca^{2+} to *E*2P formed from P_i without Ca^{2+}.** Microsomes expressing the wild-type or mutant SERCA1a were phosphorylated with $^{32}P_i$ at 25 °C for 10 min in 2.5 μl of a mixture containing 1 μg of microsomal protein, 0.1 mM $^{32}P_i$, 1 μM A23187, 1 mM EGTA, 10 mM $MgCl_2$, 50 mM MOPS/Tris (pH 7.0), and 35% (v/v) Me_2SO. The mixture was cooled and diluted at 0 ºC with 22.5 μl of the "Ca-solution" containing 22.3 mM $CaCl_2$ (to give 20 mM Ca^{2+}), 1 μM A23187, 111 mM KCl, 7 mM $MgCl_2$, and 50 mM MOPS/Tris (pH 7.0), and incubated for 1 min. This mixture was then further diluted 10-fold at 0 ºC by the addition of 225 μl of the "EGTA-solution" containing 44.4 mM EGTA, 1 μM A23187, 0.1 M KCl, 7 mM $MgCl_2$, and 50 mM MOPS/Tris (pH 7.0). At different times after this Ca^{2+}-removal, the *E*P decay was quenched by acid and the amounts of *E*P remaining were determined (*A*). The amounts of *E*P obtained at zero time (*i.e.* immediately before the addition of the "EGTA-solution") are normalized to 100%. It should be noted that the amount of *E*2P formed from P_i (at zero time) was comparable to that of *E*P formed from ATP and Ca^{2+} shown in Fig. 4 in the wild type and in each of the mutants (*e.g.* in the wild type, *E*2P formed from P_i was 3.45 ± 0.22 nmol/mg SERCA1a protein (n = 4) and *E*P formed from ATP was 3.31 ± 0.14 nmol/mg of the SERCA1a protein (n = 4)). (*B*) for determination of the ADP-insensitive *E*P, an equal volume (250 μl) of a mixture containing 4 mM ADP, 1 μM A23187, 0.1 M KCl, 7 mM $MgCl_2$, 10 mM EGTA, and 50 mM MOPS/Tris (pH 7.0) was added to the above EGTA-diluted phosphorylation mixture at the indicated time. At 1 s after this addition, the reaction was quenched by acid. The amount of the ADP-insensitive *E*P determined at each of the indicated time is shown as percentage of the total amount of *E*P determined at zero time.

FIGURE 10. A**ccessibility of lumenal Ca^{2+} in *E*2P formed from P_i without Ca^{2+}.** Microsomes expressing the wild type (*A*) or the mutant 2Gi-46/47 (*B*) were phosphorylated with $^{32}P_i$ in 2.5 μl of a mixture as described in Fig. 9. The mixture was then cooled and diluted 100-fold at 0 ºC with 247.5 μl of a solution containing various concentrations of $CaCl_2$ in 1 μM A23187, 101 mM KCl, 1 mM EGTA, 7 mM $MgCl_2$, and 50 mM MOPS/Tris (pH 7.0) to give the final Ca^{2+} concentrations as indicated with different symbols. The amount of *E*P remaining at the indicated time after this Ca^{2+} addition was determined and shown as percentage of the amount of *E*P at zero time, which was determined immediately before the Ca^{2+}-addition. The *E*P decay occurred in two phases. The first and rapid phase completed within a few seconds corresponding to the hydrolysis of *E*2P without bound Ca^{2+} (see Fig. 7). Essentially the same results were observed in the mutants 3Gi-46/47 and 4Gi-46/47 (data not shown) as in 2Gi-46/47. In *C*, the content of *E*P in the slow and second phase at each Ca^{2+} concentration was obtained by extrapolating to the zero time and plotted versus the Ca^{2+} concentration. $K_{0.5}$ for the Ca^{2+} activation and Hill coefficient obtained by fitting to the Hill equation (*solid lines*) were 1.4 mM and 1.5 (wild type), 1.3 mM and 1.5 (1Gi-46/47), 1.2 mM and 1.4 (2Gi-46/47), 1.0 mM and 1.2 (3Gi-46/47), 0.9 mM and 1.4 (4Gi-46/47), as summarized in Table I.

FIGURE 11. **Thapsigargin accelerates the decay of *E*2PCa_2 accumulated with the mutant.** (●, ▲); microsomes expressing the mutant 4Gi-46/47 were phosphorylated with [γ-^{32}P]ATP and Ca^{2+} at 25 ºC in 25 μl of the mixture otherwise as described in the legend to Fig. 6. (○, Δ); microsomes expressing the mutant 4Gi-46/47 were phosphorylated with $^{32}P_i$ in 2.5 μl of a mixture, and then diluted at 25 ºC with 22.5 μl of the "Ca-solution" containing 22.3 mM $CaCl_2$, 1 μM A23187, 111 mM KCl, 7 mM $MgCl_2$, and 50 mM MOPS/Tris (pH 7.0), and incubated for 1 min, otherwise as described in the legend for Fig. 9. Both of the above phosphorylation mixtures were then diluted 10-fold at 25 ºC by addition of 225 μl of the EGTA-solution containing 44.4 mM EGTA, 1 μM A23187, 0.1 M KCl, 7 mM $MgCl_2$, and 50 mM MOPS/Tris (pH 7.0) in the absence (●, ○) or presence (▲, Δ) of 1 μM thapsigargin (TG). At different times after this dilution, the amount of *E*P remaining was determined by the acid-quenching.

FIGURE 12. **Structural analysis of major intermediates and *E*2PCa$_2$ by limited proteolysis.** The major intermediates of the transport cycle and their structural analogs were produced with the wild type (*upper panels*) and the mutant 4Gi-46/47 (*lower panels*) in the microsomes (0.1 mg/ml) under the conditions described below, and subjected to the limited proteolysis with 0.5 mg/ml trypsin (*A*) or PrtK (*B*) at 25 °C for the indicated time periods. The proteolysis was terminated by 2.5% (v/v) trichloroacetic acid, and the digests were subjected to Laemmli SDS-PAGE. The ATPase chain and its fragments separated on the gel were blotted onto a polyvinylidene fluoride membrane and visualized by immunodetection with a monoclonal antibody that recognizes the Ala^{199}-Arg^{505} peptide (tryptic fragment "A1") of SERCA1a, as described under "Experimental Procedures." The *E*2 state was produced in 5 mM EGTA, 0.1 M KCl, 7 mM $MgCl_2$, 1 μM A23187, and 50 mM MES/Tris (pH 6.0). The *E*1Ca$_2$ state was produced in 0.1 mM $CaCl_2$, 0.1 M KCl, 7 mM $MgCl_2$, 1 μM A23187, and 50 mM MOPS/Tris (pH 7.0). To produce the *E*1·AlF$_x$·ADP complex (*E*1PCa$_2$·ADP analog), the microsomes were incubated at 25 °C for 40 min in 50 μM $AlCl_3$, 3 mM KF, 0.1 mM ADP, 0.1 M KCl, 0.1 mM $CaCl_2$, 7 mM $MgCl_2$, 1 μM A23187, and 50 mM MOPS/Tris (pH 7.0), and then the protease was added. For the *E*P formation from ATP, the microsomes were incubated at 25 °C for 10 s in 0.5 mM ATP, 0.1 M KCl, 7 mM $MgCl_2$, 5 mM $CaCl_2$, 1 μM A23187, and 50 mM MOPS/Tris (pH 7.0), and then the protease was added. In the wild type, *E*P accumulated was exclusively *E*1PCa$_2$ and its decay was extremely slowed during the proteolysis periods due to the feedback inhibition by the high concentration of Ca^{2+}. In the mutant, *E*P accumulated was exclusively *E*2PCa$_2$ and its decay was extremely slow, as demonstrated in Figs. 6 and 8. The same results were obtained in 0.1 mM Ca^{2+} as in 5 mM Ca^{2+} in the mutant (data not shown). To produce the *E*2·AlF_4^- complex (the transition state analog of the *E*2P hydrolysis (17)), the microsomes were preincubated at 25 °C for 40 min in 50 μM $AlCl_3$, 3 mM KF, 0.1 M KCl, 5 mM EGTA, 7 mM $MgCl_2$, 1 μM A23187, and 50 mM MES/Tris (pH 6.0). For producing *E*2V$_i$ (the *E*2P analog (15)), the microsomes were preincubated with 0.1 mM orthovanadate in 50 mM MOPS/Tris (pH 7.0) instead of 50 μM $AlCl_3$/3 mM KF in 50 mM MES/Tris (pH 6.0), otherwise as above. The tryptic fragments; "A", Met^1-Arg^{505}; and "A1", Ala^{199}-Arg^{505}. The fragments formed by PrtK; "p95", Lys^{120}-Gly^{994}; "p81", Met^1-Met^{733}; and "p83", Glu^{243}-Gly^{994} (48, 49). The positions of the Ca^{2+}-ATPase chain and its fragments, and those of the molecular mass markers are indicated on the left and right margins, respectively. Note also that the antibody immunodecorated trypsin (*A*) and PrtK (*B*), in addition to the Ca^{2+}-ATPase fragments.

FIGURE 13. **Detailed structural model for the change *E*1PCa$_2$ → *E*2P + 2Ca^{2+}.** The coordinates for the structures *E*1·AlF$_x$·ADP and *E*2·MgF_4^{2-} were obtained from the Protein Data Bank (accession code 1WPE and 1WPG, respectively (13)). The two structures were manually fitted with M8-M10, which do not move virtually in the two structures. The A and P domains are *yellow* and *pink*, respectively. The N domain and ADP are not depicted for simplicity. The junctions of the N domain with the P domain are indicated by "*To N*" and "*From N*". *M4C* and *M4L* are the cytoplasmic and lumenal parts of M4, respectively. The A/M1-linker (Glu^{40}-Ser^{48}) is *red*. The phosphorylation site (Asp^{351}), and the bound P_i analogs AlF_x and MgF_4^{2-} (*blue spheres* (fluoride) with *white* or *magenta sphere* (aluminum or magnesium)) in *E*1·AlF$_x$·ADP and *E*2·MgF_4^{2-} are shown. *Yellow solid arrow* on *E*1·AlF$_x$·ADP indicates the movement of the A domain in the change *E*1·AlF$_x$·ADP → *E*2·MgF_4^{2-} (*i.e.* rotation by ~110° approximately parallel to the membrane plane). *Dashed arrows* with *red*, *blue*, and *green* on *E*2·MgF_4^{2-} indicate the approximate change of the position of the P_i analog (*red*), rotation of M1' (*blue*), and tilting of M2 (*green*) in the change *E*1·AlF$_x$·ADP → *E*2·MgF_4^{2-}. Note that the P domain tilts significantly with the connected M4/M5 toward the bottom part of the A domain, and that the V-shaped rigid body structure formed by M1'/M1 and M2 largely tilts. These rearrangements of the transmembrane helices were predicted to result in the Ca^{2+} release into lumen (13). *T2*, the tryptic site Arg^{198} on the Val^{200} loop (Asp^{196}-Asp^{203}, *blue*); *PrtK*, the sites for proteinase K (Leu^{119} on the top part of M2 (A/M2-linker region), Thr^{242} on the A/M3-linker, and Ala^{746} on M5). In *E*2·MgF_4^{2-}, the A and P domains are associated by their interactions at three regions (*semitransparent purple, blue,*

and *orange spheres*) as also depicted in Fig. 2. The Tyr^{122}-hydrophobic cluster (*orange* region) is formed from the A domain ($Ile^{179/}Leu^{180}/Ile^{232}$), the P domain ($Val^{705}/Val^{726}$), and the top part of M2 (Tyr^{122}/Leu^{119}). The $T^{181}GES$ loop (*purple* region) forms a hydrogen-bonding network with the residues of the P domain around Asp^{351}; the Val^{200} loop (*blue* region) forms an ionic and hydrogen-bonding network with the polar residues of the P domain ($Arg^{678}/Glu^{680}/Arg^{656}/Asp^{660}$). Details of these interaction networks are not depicted for simplicity (see Supplemental Figures in Ref. 19 for the detailed structures of the interaction networks). Note that the associations between the A and P domains at the Val^{200} loop and at the Tyr^{122}-hydrophobic cluster are definitely monitored by the resistance due to steric hindrance of Arg^{198} against trypsin and that of Leu^{119} against proteinase K, respectively (15-17).

TABLE I

Kinetic parameters determined for partial reaction steps

The affinity of the transport sites for Ca^{2+} ($K_{0.5}$) and the Hill coefficient (n) in the $E2$ to $E1Ca_2$ transition were determined at 0 °C by the EP formation from ATP in the presence of various concentrations of Ca^{2+} under the conditions otherwise as described in the legend to Fig. 4 and by the least square fit to the Hill equation. The rate of the $E2$ to $E1Ca_2$ transition in steps 1-2 were determined by the $E1PCa_2$ formation from the $E2$ state upon the simultaneous addition of saturating 100 μM Ca^{2+} and ATP at pH 6.0 under the conditions otherwise as in Fig. 4. In this EP formation, the $E2$ to $E1Ca_2$ transition is rate-limiting. The rates for the other steps were obtained at 0 °C in the experiments in Fig. 5*A*, *C* ($E1Ca_2$ to $E1PCa_2$ step 3), Fig. 5*B*, *D* (Loss of ADP-sensitivity (*i.e.* accumulation of ADP-insensitive EP from ADP-sensitive EP in step 4)), Fig. 6 (Decay of EP formed from ATP in the presence of Ca^{2+} (EP_{ATP})), and Fig. 7 (Hydrolysis of $E2P$ formed from P_i in the absence of Ca^{2+} ($E2P_{Pi}$) in steps 6-7). In parenthesis, the values obtained with the wild type are normalized to 100%. $E2P$ to $E2PCa_2/E1PCa_2$; the accessibility of lumenal Ca^{2+} to the transport sites of $E2P$ was assessed at 0 °C in Fig. 10 by determining the affinity for Ca^{2+} ($K_{0.5}$) and the Hill coefficient (n) in the reverse reaction, *i.e.* upon the addition of Ca^{2+} to $E2P$ and the consequent formation of $E2PCa_2$ or $E1PCa_2$ (see RESULTS with Fig. 10 for details of the formation of these stable EP species in the reverse reaction).

	$E2$ to $E1Ca_2$				$E1Ca_2$ to		Loss of			Decay of		Hydrolysis of		$E2P$ to $E2PCa_2/E1PCa_2$	
	Ca^{2+} affinity		Rate		$E1PCa_2$ [b]		ADP-sensitivity			EP_{ATP}		$E2P_{Pi}$		Ca^{2+} affinity	
	$K_{0.5}$	n			(-)K^+		(+)K^+	(-)K^+						$K_{0.5}$	n
	μM		s^{-1}	%	s^{-1}	%	s^{-1}	s^{-1}	%	s^{-1}	%	s^{-1}	%	mM	
Wild type	0.16	1.87	0.213	(100)	1.37	(100)	-[c]	0.34	(100)	0.0390	(100)	0.64	(100)	1.4	1.5
4Ai-22/23	0.18	1.65	0.292	(137)	1.30	(95)	-[c]	0.63	(188)	0.0613	(157)	1.07	(169)	2.2	1.1
1Gi-42/43	0.16	1.88	0.157	(74)	1.91	(140)	-[c]	0.53	(156)	0.0247	(63)	1.07	(169)	2.3	1.5
4Gi-42/43	0.13	1.73	0.131	(62)	2.01	(147)	2.90[d]	1.70[d]	(504)	0.0003	(0.9)	0.62	(98)	0.9	1.4
1Gi-46/47	0.16	1.74	0.147	(69)	1.09	(80)	-[c]	0.32	(95)	0.0194	(50)	1.08	(170)	1.3	1.5
2Gi-46/47	0.13	1.68	0.208	(97)	1.30	(95)	0.92	0.61	(180)	0.0006	(1.5)	0.79	(124)	1.2	1.4
3Gi-46/47	0.15	1.50	0.239	(112)	1.80	(131)	2.83[d]	1.70[d]	(504)	0.0001	(0.2)	0.85	(134)	1.0	1.2
4Gi-46/47	0.14	2.07	0.226	(106)	1.94	(142)	3.71[d]	1.95[d]	(578)	0.0001	(0.3)	0.90	(142)	0.9	1.4
6Gi-46/47	0.15	1.48	0.136	(64)	4.20	(307)	4.37[d]	3.56[d]	(1054)	0.0001	(0.2)	0.75	(118)	0.9	1.2
4Ai-53/54	0.29	1.70	0.428	(201)	2.26	(165)	-[c]	0.48	(143)	0.0288	(74)	0.60	(94)	1.1	1.4
4950525354S	-		-[a]		0.12	(9.1)	-	0.08[e]	(24)	0.0060	(15)	1.08	(170)	-	-
5155565859A	0.22	1.82	0.562	(264)	1.02	(75)	-[c]	0.33	(97)	0.0312	(80)	0.84	(132)	0.7	1.3

[a] Not determined because the *E*P formation from $E1Ca_2$ was slow (see Fig. 5*A*).
[b] The rate of the $E1PCa_2$ formation from $E1Ca_2$ in the presence of K^+ was very similar to that in the absence of K^+ (see Fig. 5*A* and *C*), therefore not shown for simplicity.
[c] Not determined because the accumulation of ADP-insensitive *E*P was low.
[d] The rate of the *E*P isomerization (loss of the ADP-sensitivity) must be faster because almost all of *E*P formed had become already ADP-insensitive during the *E*P formation (see Fig. 5).
[e] The apparent slow rate is probably due to the slowed *E*P formation from $E1Ca_2$ and ATP. The rate of the *E*P isomerization (loss of the ADP-sensitivity) must be faster because a very large fraction of *E*P formed had become already ADP-insensitive during the *E*P formation (see Fig. 5).

Figure 1

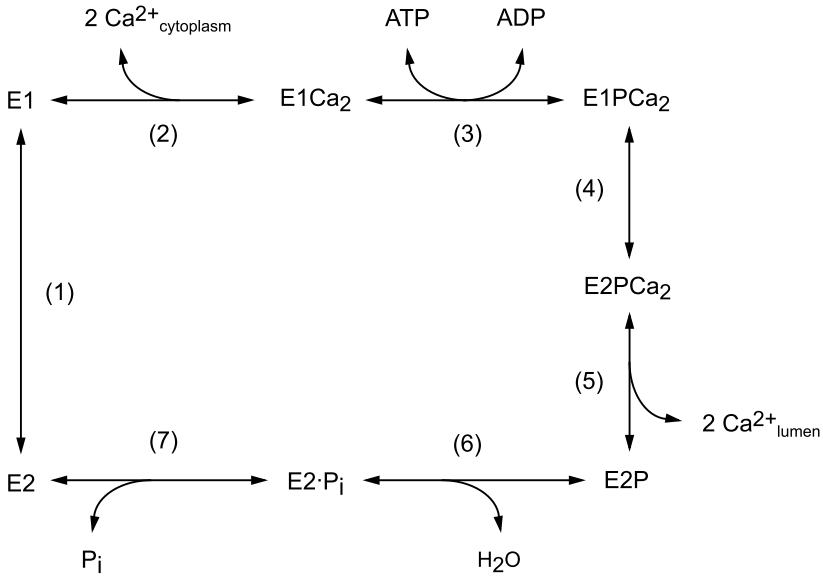
2 Ca2+cytoplasm
ATP
ADP
E1
E1Ca2
E1PCa2
(2)
(3)
(4)
(1)
E2PCa2
(5)
2 Ca2+lumen
(7)
(6)
E2
E2·Pi
E2P
Pi
H2O

Figure 2

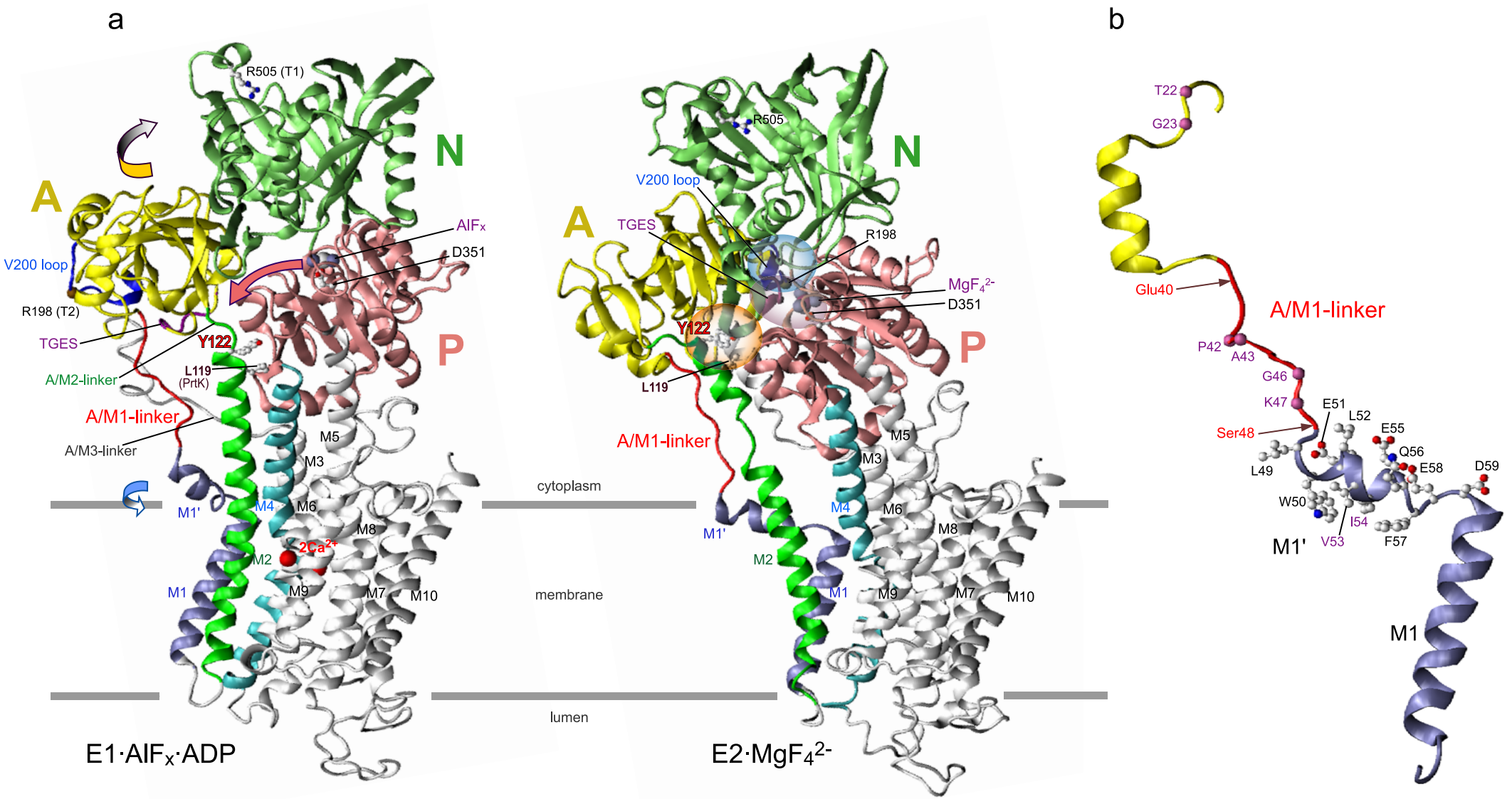
a
b
R505 (T1)
N
A
P
AlFx
D351
V200 loop
R198 (T2)
TGES
Y122
L119
(PrtK)
A/M2-linker
A/M1-linker
A/M3-linker
M5
M3
M4
M6
M8
M1'
2Ca2+
M2
M1
M9
M7
M10
cytoplasm
membrane
lumen
E1·AlFx·ADP
R505
V200 loop
TGES
R198
MgF4 2-
D351
Y122
L119
A/M1-linker
E2·MgF4 2-
T22
G23
Glu40
A/M1-linker
P42
A43
G46
K47
E51
L52
Ser48
E55
Q56
L49
E58
D59
W50
I54
V53
F57
M1'
M1

Figure 3

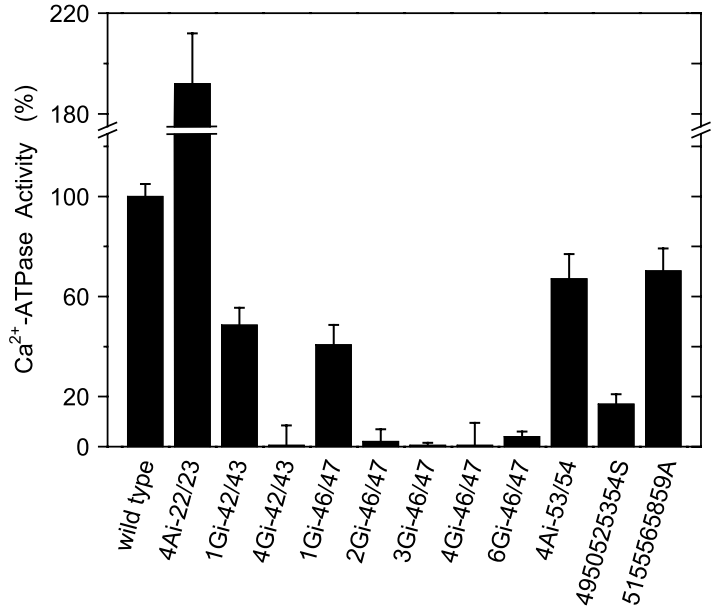
220
180
100
60
20
0
Ca2+-ATPase Activity (%)
wild type
4Ai-22/23
1Gi-42/43
4Gi-42/43
1Gi-46/47
2Gi-46/47
3Gi-46/47
4Gi-46/47
6Gi-46/47
4Ai-53/54
4950525354S
5155565859A

Figure 4

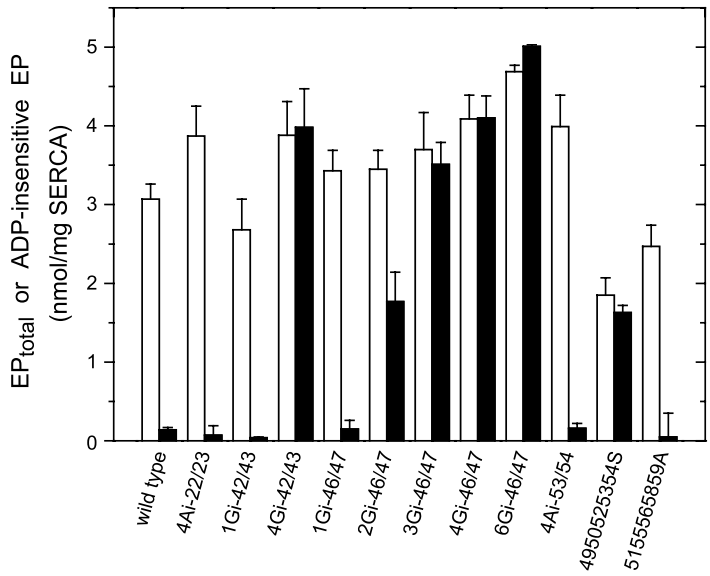
EP$_{total}$ or ADP-insensitive EP
(nmol/mg SERCA)
0
1
2
3
4
5
wild type
4Ai-22/23
1Gi-42/43
4Gi-42/43
1Gi-46/47
2Gi-46/47
3Gi-46/47
4Gi-46/47
6Gi-46/47
4Ai-53/54
4950525354S
5155565859A

Figure 5

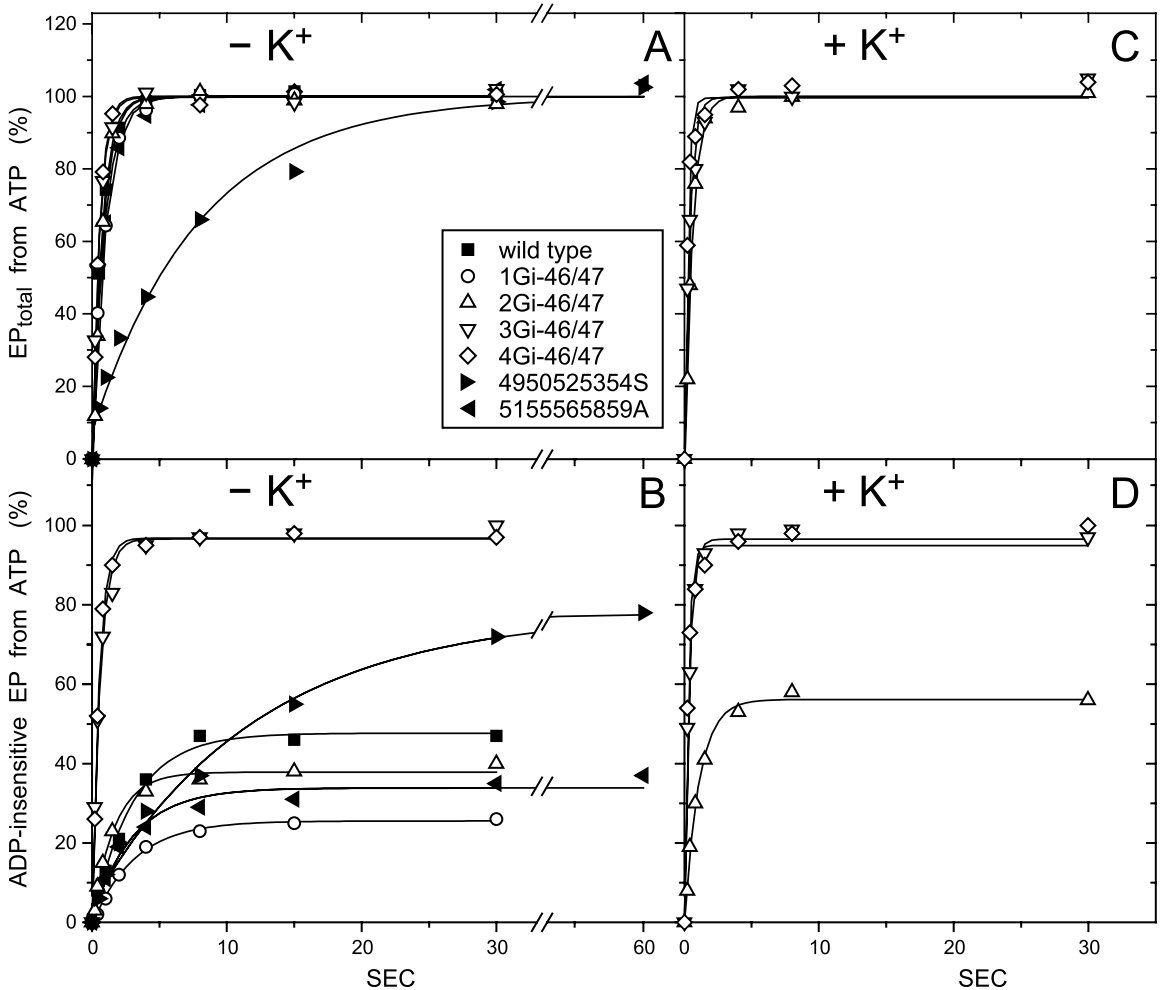
− K+
A
+ K+
C
− K+
B
+ K+
D
EPtotal from ATP (%)
ADP-insensitive EP from ATP (%)
wild type
1Gi-46/47
2Gi-46/47
3Gi-46/47
4Gi-46/47
4950525354S
5155565859A
SEC
SEC

Figure 6

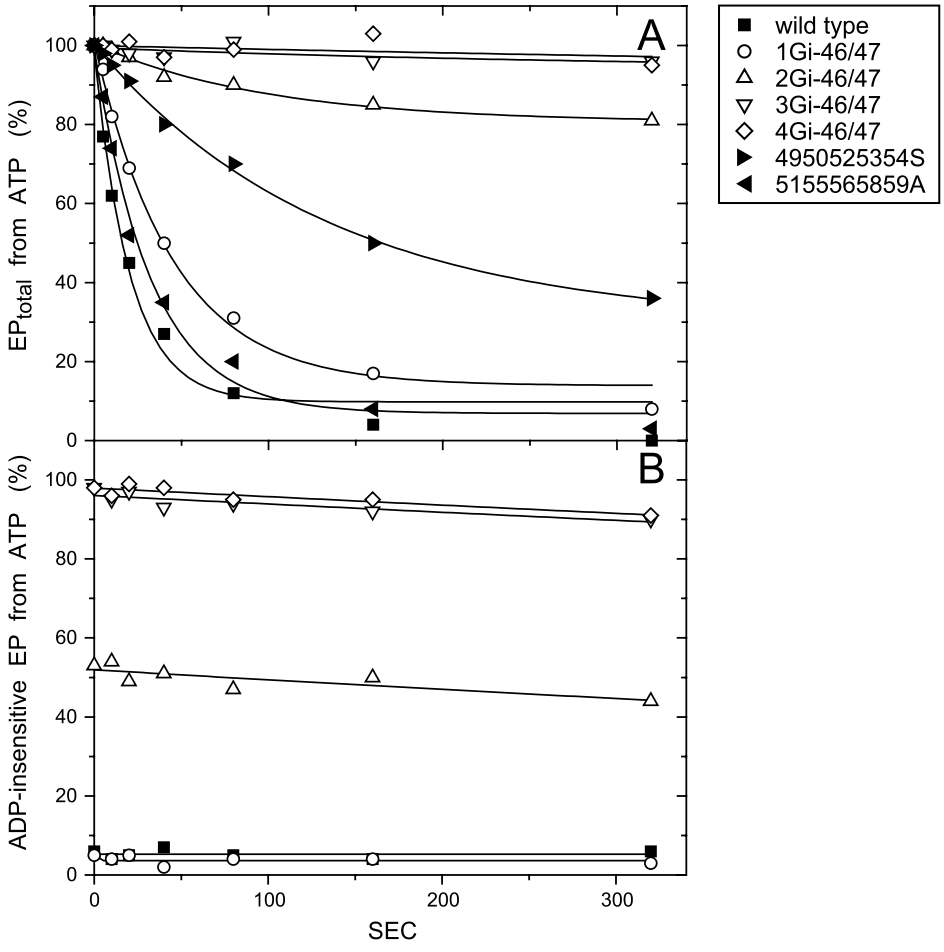
A
B
wild type
1Gi-46/47
2Gi-46/47
3Gi-46/47
4Gi-46/47
4950525354S
5155565859A
EP$_{total}$ from ATP (%)
ADP-insensitive EP from ATP (%)
SEC
0
20
40
60
80
100
0
100
200
300

Figure 7

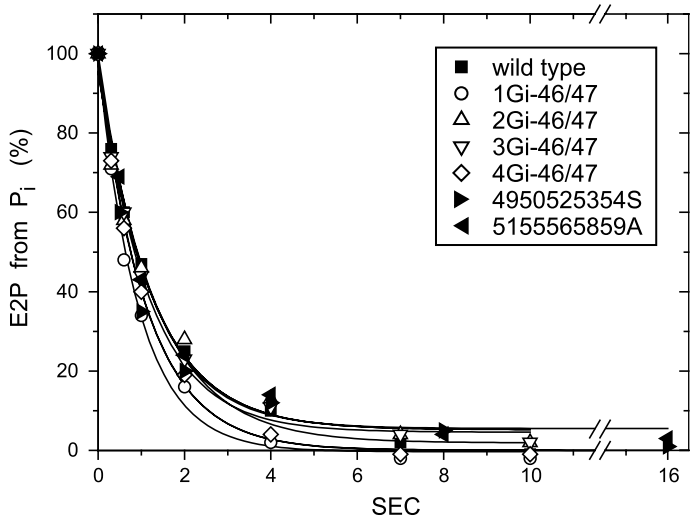
E2P from P_i (%)
SEC
wild type
1Gi-46/47
2Gi-46/47
3Gi-46/47
4Gi-46/47
4950525354S
5155565859A
0
20
40
60
80
100
0
2
4
6
8
10
16

Figure 8

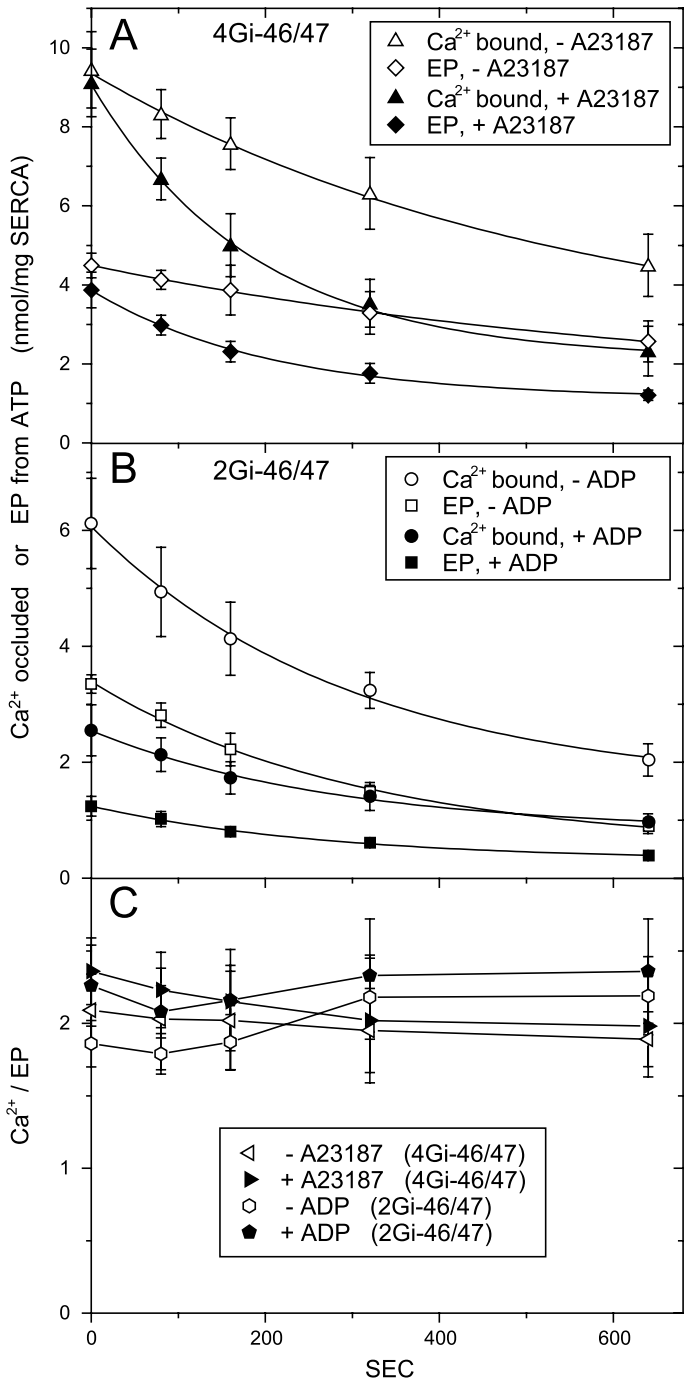
A
4Gi-46/47
Ca2+ bound, - A23187
EP, - A23187
Ca2+ bound, + A23187
EP, + A23187
B
2Gi-46/47
Ca2+ bound, - ADP
EP, - ADP
Ca2+ bound, + ADP
EP, + ADP
C
- A23187 (4Gi-46/47)
+ A23187 (4Gi-46/47)
- ADP (2Gi-46/47)
+ ADP (2Gi-46/47)
Ca2+ occluded or EP from ATP (nmol/mg SERCA)
Ca2+ / EP
SEC
0
200
400
600
0
2
4
6
8
10
1

Figure 9

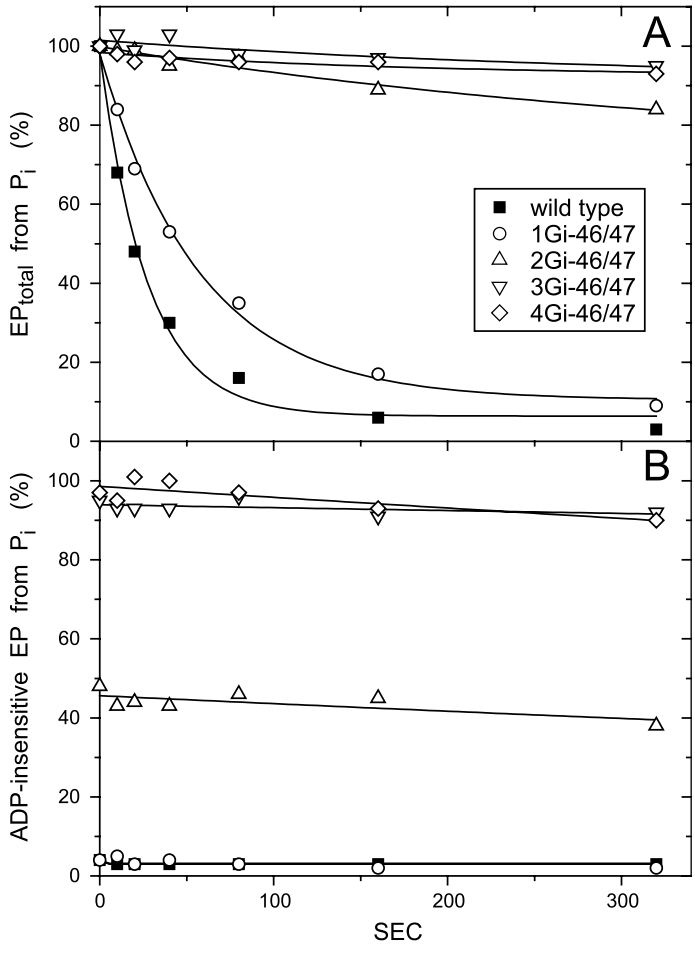
A
B
wild type
1Gi-46/47
2Gi-46/47
3Gi-46/47
4Gi-46/47
EP$_{total}$ from P$_i$ (%)
ADP-insensitive EP from P$_i$ (%)
0
20
40
60
80
100
0
100
200
300
SEC

Figure 10

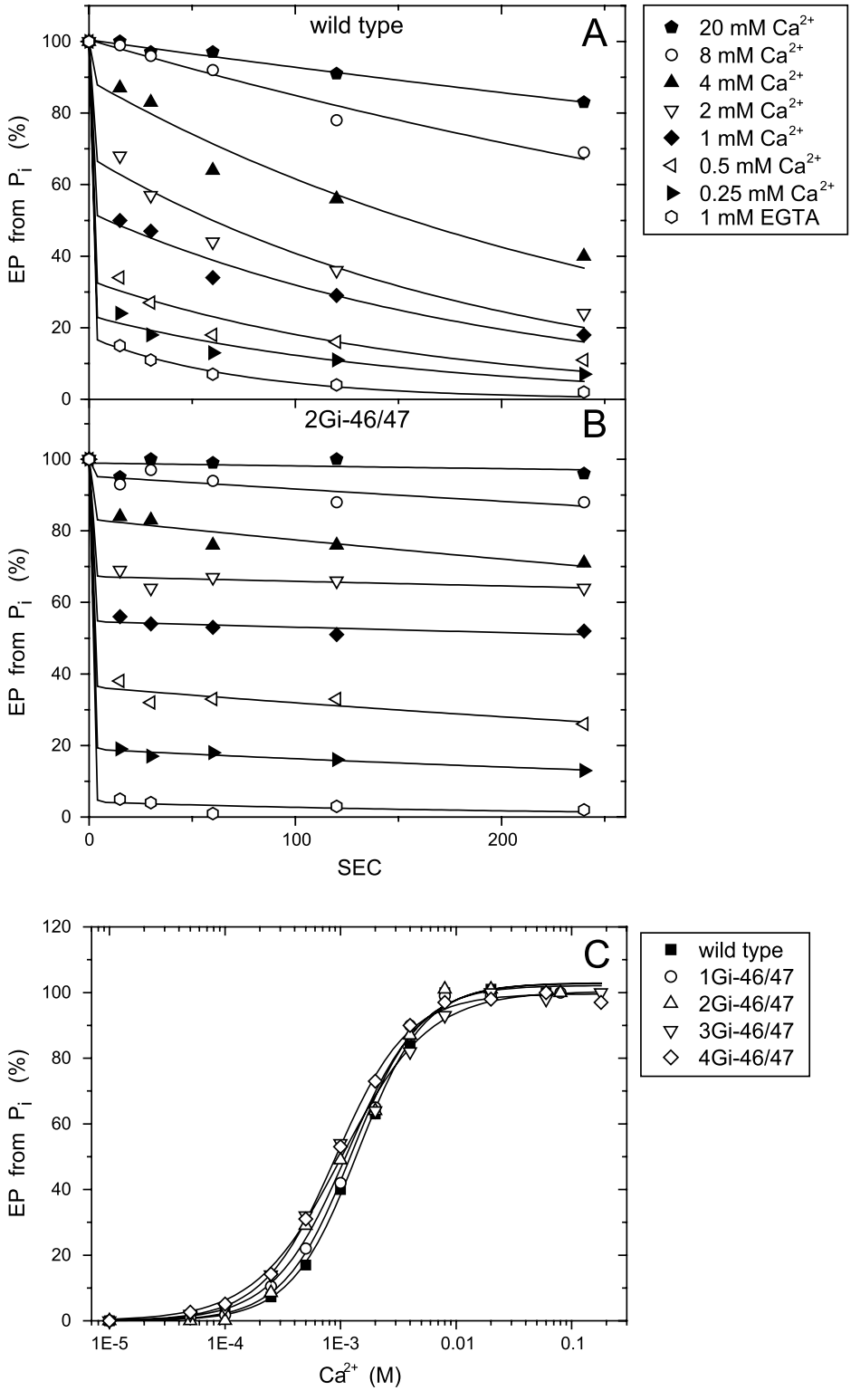
wild type
A
2Gi-46/47
B
EP from P_i (%)
SEC
20 mM Ca^{2+}
8 mM Ca^{2+}
4 mM Ca^{2+}
2 mM Ca^{2+}
1 mM Ca^{2+}
0.5 mM Ca^{2+}
0.25 mM Ca^{2+}
1 mM EGTA
C
wild type
1Gi-46/47
2Gi-46/47
3Gi-46/47
4Gi-46/47
Ca^{2+} (M)

Figure 11

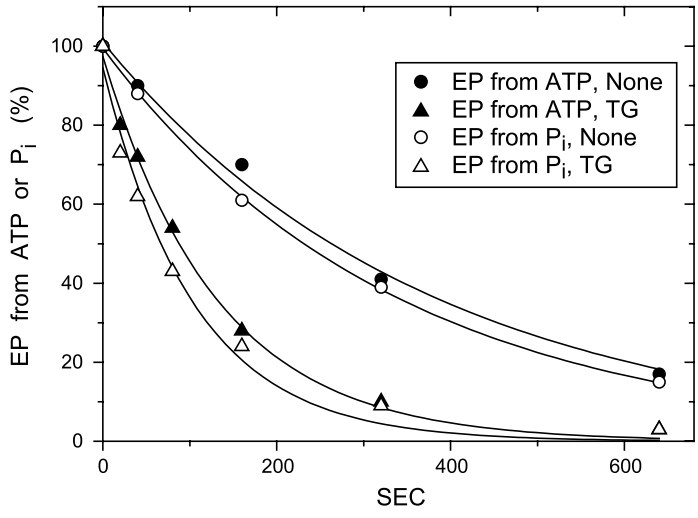
EP from ATP, None
EP from ATP, TG
EP from Pi, None
EP from Pi, TG
EP from ATP or Pi (%)
SEC
0
20
40
60
80
100
0
200
400
600

Figure 12A

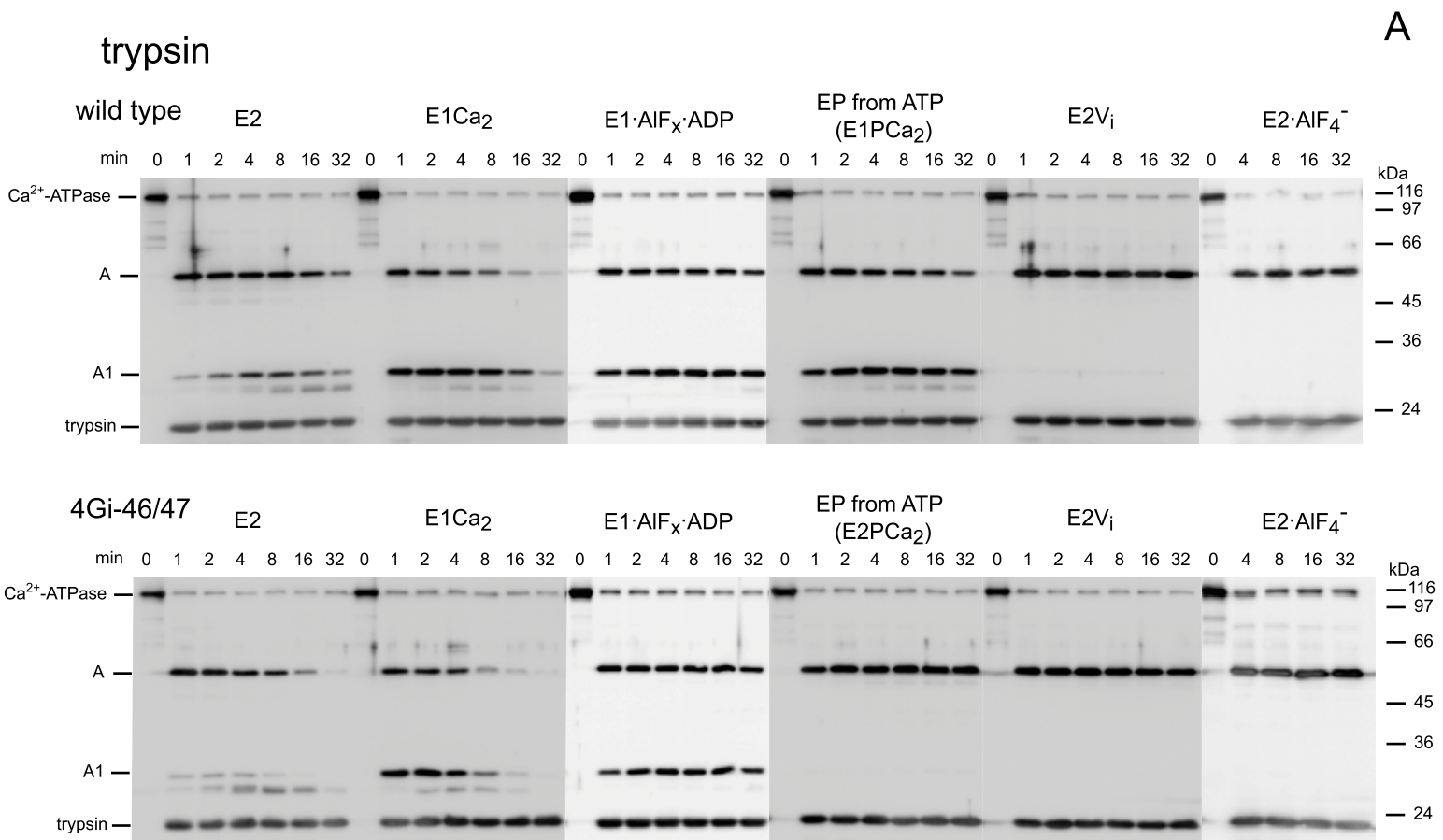
A
trypsin
wild type
E2
E1Ca2
E1·AlFx·ADP
EP from ATP
(E1PCa2)
E2Vi
E2·AlF4-
min 0 1 2 4 8 16 32 0 1 2 4 8 16 32 0 1 2 4 8 16 32 0 1 2 4 8 16 32 0 1 2 4 8 16 32 0 4 8 16 32
Ca2+-ATPase
A
A1
trypsin
kDa
116
97
66
45
36
24
4Gi-46/47
E2
E1Ca2
E1·AlFx·ADP
EP from ATP
(E2PCa2)
E2Vi
E2·AlF4-
min 0 1 2 4 8 16 32 0 1 2 4 8 16 32 0 1 2 4 8 16 32 0 1 2 4 8 16 32 0 1 2 4 8 16 32 0 4 8 16 32
Ca2+-ATPase
A
A1
trypsin
kDa
116
97
66
45
36
24

Figure 12B

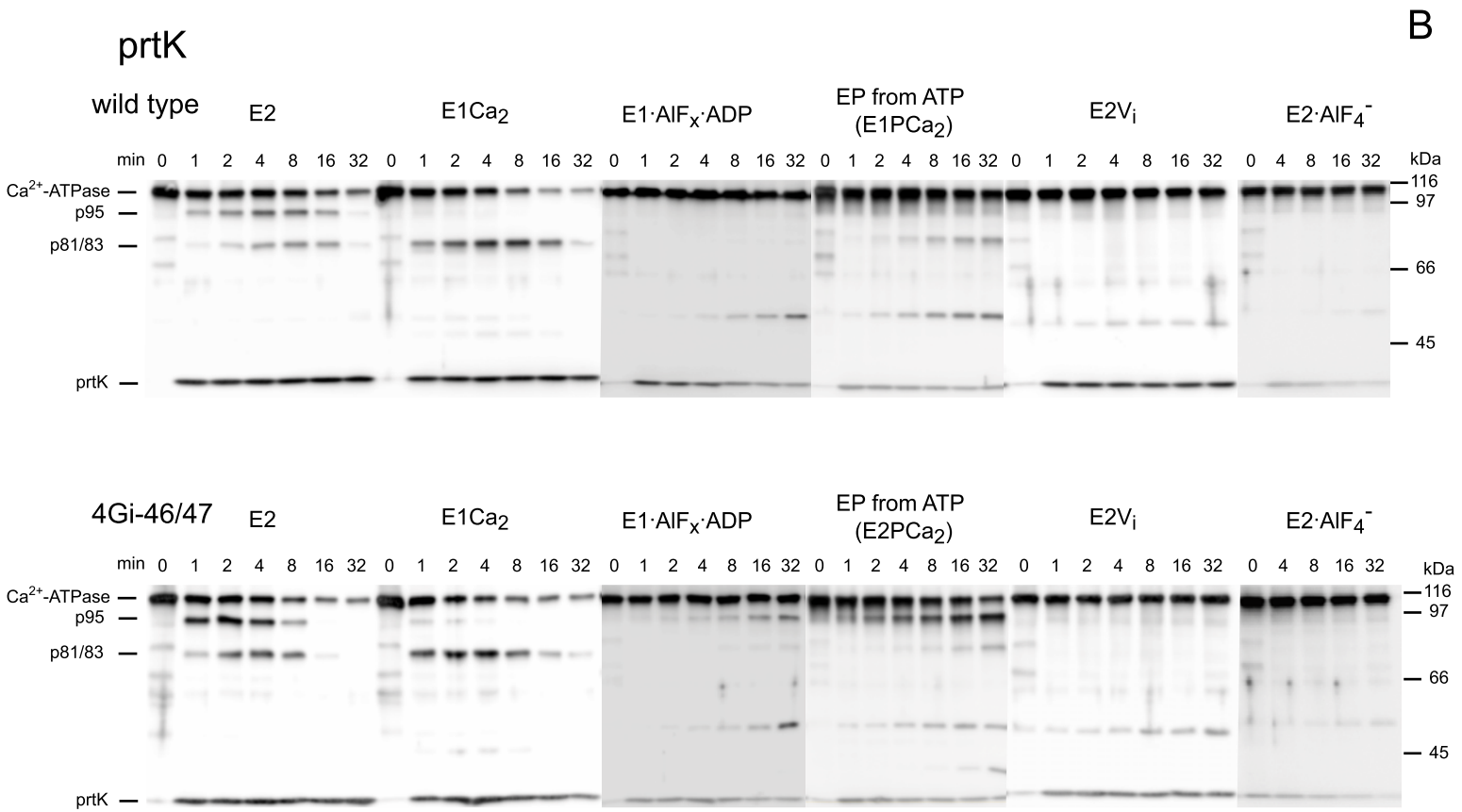
prtK
B
wild type
E2
E1Ca2
E1·AlFx·ADP
EP from ATP (E1PCa2)
E2Vi
E2·AlF4-
min 0 1 2 4 8 16 32 0 1 2 4 8 16 32 0 1 2 4 8 16 32 0 1 2 4 8 16 32 0 1 2 4 8 16 32 0 4 8 16 32
kDa
Ca2+-ATPase
p95
p81/83
prtK
116
97
66
45
4Gi-46/47
E2
E1Ca2
E1·AlFx·ADP
EP from ATP (E2PCa2)
E2Vi
E2·AlF4-
min 0 1 2 4 8 16 32 0 1 2 4 8 16 32 0 1 2 4 8 16 32 0 1 2 4 8 16 32 0 1 2 4 8 16 32 0 4 8 16 32
kDa
Ca2+-ATPase
p95
p81/83
prtK
116
97
66
45

Figure 13

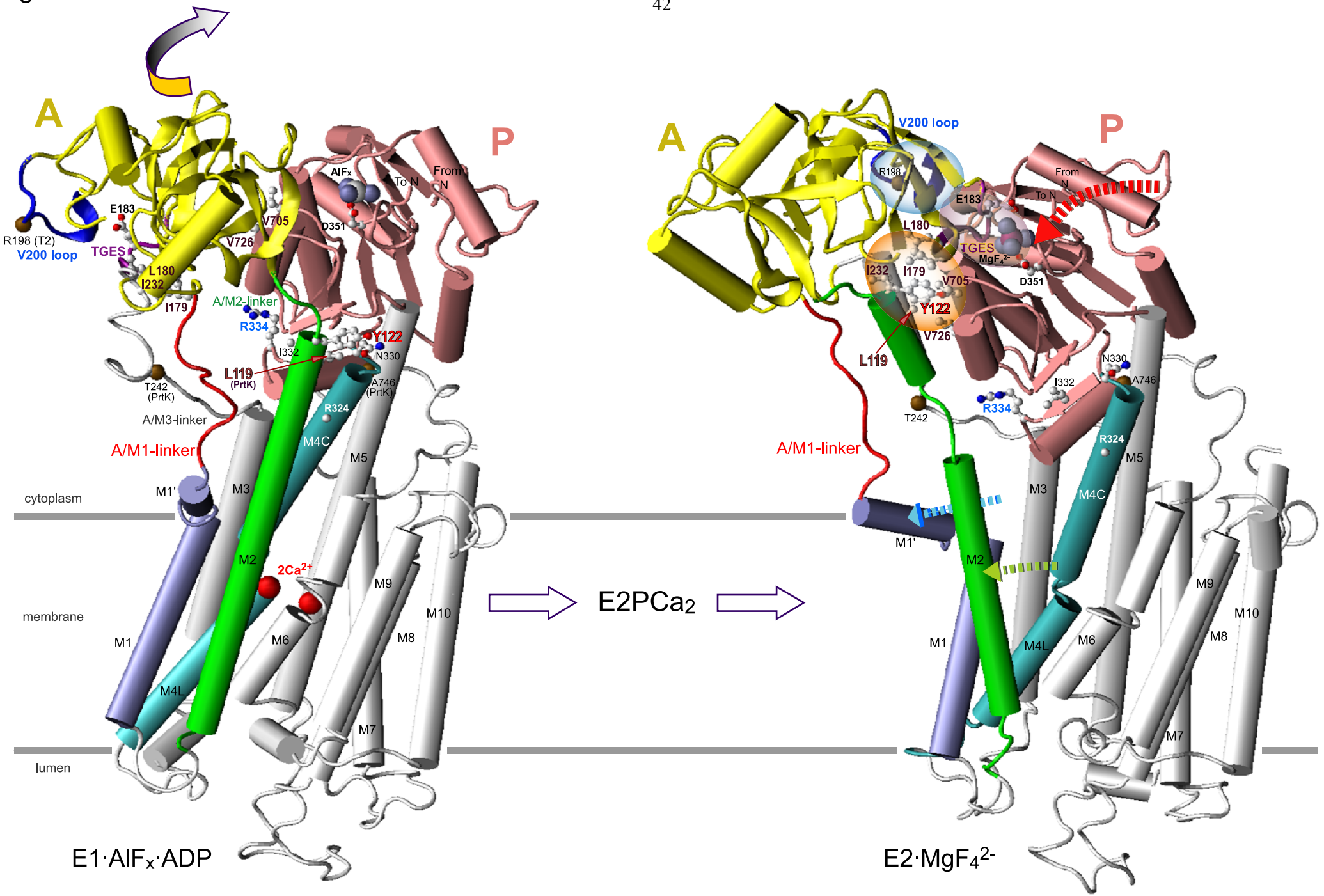
A
P
V200 loop
R198 (T2)
E183
TGES
L180
I232
I179
V705
V726
AlFx
D351
To N
From N
A/M2-linker
R334
I332
Y122
N330
L119
(PrtK)
T242
(PrtK)
A746
(PrtK)
R324
A/M3-linker
A/M1-linker
M4C
M5
M1'
M3
M2
2Ca2+
M9
M10
M6
M8
M1
M4L
M7
cytoplasm
membrane
lumen
E1·AlFx·ADP
E2PCa2
A
P
V200 loop
R198
E183
L180
TGES
MgF4 2-
I232
I179
V705
D351
Y122
V726
L119
From N
To N
N330
A746
I332
R334
T242
A/M1-linker
R324
M5
M3
M4C
M1'
M2
M9
M10
M1
M4L
M6
M8
M7
E2·MgF4 2-